ELSEVIER

Chemical Geology 169 (2000) 157–185

CHEMICAL GEOLOGY
INCLUDING
ISOTOPE GEOSCIENCE

www.elsevier.com/locate/chemgeo

Neodymium isotopes in basalts of the southwest basin and range and lithospheric thinning during continental extension

Donald J. DePaolo [*,1], E. Ellen Daley

Center for Isotope Geochemistry, Department of Earth and Planetary Science, University of California, Berkeley, CA 94720-4767, USA

Received 31 March 1999; accepted 15 March 2000

Abstract

The chemical compositions, ages, and Nd and Sr isotopic compositions of Miocene basaltic volcanic rocks from the southwestern Basin and Range Province were measured. The data presented, and other data obtained from the literature show that temporal variations in the Nd and Sr isotopic compositions are typically correlated with the timing of local crustal extension. The isotopic variations cannot be accounted for by crustal contamination, and are best interpreted as indicating the involvement of subcontinental lithospheric mantle as a major source of basalt magma before and during the early stages of extension, giving way to asthenospheric sources as extension proceeds. It is inferred that the basalt isotopic and age data provide information about the amount and timing of changes of the overall lithosphere thickness during extension. If this inference is valid, the inferred lithosphere thickness vs. time histories can be compared to the amount and timing of upper crustal extension to evaluate competing models for lithospheric strain during continental extension.

The depth of the lithosphere–asthenospshere boundary is inferred primarily from the isotopic data, but can be refined by accounting for differences in the depth of origin of the basalts as suggested by differences in the degree of silica saturation (nepheline normative vs. hypersthene normative). The transition between silica saturated and undersaturated magmas is dependent on many factors, but for the conditions likely to apply to the Basin and Range Miocene volcanism, it corresponds to a depth of origin of 50 ± 10 km.

The data presented show strong support for the inferred mantle geochemical stratigraphy, and the inferred modern depths to the lithosphere–asthenosphere boundary are consistent with available seismic refraction and structural data. In the highly extended regions near the eastern and western margins of the southwestern Basin and Range, temporal changes in basalt isotopic compositions indicate that the subjacent lithospheric mantle thinned contemporaneously with the upper crust, as would be predicted for pure shear. These areas are also characterized by relatively high (although still low) basalt extrusion rates. In contrast, upper crustal extension in the Death Valley area was not accompanied by significant thinning of the subjacent lithospheric mantle, which implies that the location of lithospheric thinning was offset from the location of upper crustal extension as in a simple shear model. The total amount of lithospheric thinning is generally less than would be

[*] Corresponding author. Department of Earth and Planetary Science, University of California, McCone Hall MS4767, Berkeley, CA 94720-4767, USA. Fax: +1-510-642-9520.

E-mail address: depaolo@socrates.berkeley.edu (D.J. DePaolo).

[1] Also at Earth Sciences Division, E.O. Lawrence Berkeley National Laboratory, Berkeley, CA 94720, USA.

PII: S0009-2541(00)00261-8

expected from the magnitude of upper crustal extension and is more evenly distributed; this suggests that there is also a component of distributed shear.

Keywords: Isotopes; Basalts; Lithospheric thinning

1. Introduction

This study examines the isotopic geochemistry of Miocene-to-Recent basalts from the southwestern Basin and Range region, and attempts a synthesis that accounts for both the spatial and temporal variations. The underlying principle is that isotopic and trace element geochemistry of basalt reflects the state of the mantle lithosphere and asthenosphere at depths of about 40 to 100 km where the magmas originate. The geochemical information, because it relates to the deeper lithosphere, is therefore complementary to the information obtained from traditional structural studies based on surficial geology. Geochemistry also augments geophysical investigations, which address the current state of the extensional region but give little information on the prior intermediate states of the system.

The objective of this study is to determine whether basalt geochemistry can be used to determine the depth to the base of the lithosphere, and how that depth changed locally over the past 20 million years or so in the southwest Basin and Range province. This requires that basaltic volcanism accompany the extension and be widely distributed in space and time, that the lithosphere be geochemically distinct from the underlying asthenospheric mantle, and that the depth of origin of the basalt magmas can be estimated. The first of these requirements is met to a fair degree in the Basin and Range. There is ample evidence of the geochemical distinctiveness of the lithosphere, discussed below. And there are abundant data pertaining to the depth of origin of basalts even though there is still substantial uncertainty in applying those data to individual lava flows. The approach taken here is to accept the geochemical distinction of the continental lithosphere, use a model for the depth of origin of the basalts based on their chemical compositions, and to investigate the implications for the attenuation of the lithosphere during extension. Although there are uncertainties and this approach will require further refinement in the future, the approach does appear promising, if not necessary, to understand the geochemistry of continental volcanism.

Synopses of the many studies of upper crustal deformation in the southern Basin and Range (Wernicke et al., 1988; and references therein; also Spencer and Reynolds, 1991, for west central Arizona) provide the structural framework for interpretation of the basalt data. There is an extensive literature on basalt chemistry and isotopic composition in the Basin and Range of the western U.S. (e.g. Ormerod et al, 1988; Farmer, 1988; Farmer et al., 1989, 1995; Lum et al., 1989; Kempton et al., 1991; Fitton et al., 1988, 1991; Menzies, 1989; Menzies and Kyle, 1990; Johnson, 1991; Daley and DePaolo, 1992; Bradshaw et al., 1993; Feuerbach et al., 1993; Rogers et al., 1995; Reid and Ramos, 1996; Beard and Johnson, 1997). In this study we augment the existing data base so that there is coverage of most of the SW Basin and Range, which allows us to evaluate the large scale space-time patterns in terms of models for lithospheric attenuation associated with extension. This study emphasizes the temporal changes in isotopic composition in particular, an element of the regional variability that has received less attention than the spatial variations. All of the isotopic data used in this work, including data from the literature, were obtained on lava flows that have been dated by the K–Ar method.

From geometric considerations, thinning of the lithosphere must accompany continental extension. Predictions of where lithospheric thinning occurs in relation to upper crustal deformation vary widely depending on how strain is transmitted through the lithosphere (Fig. 1; e.g. Buck et al., 1988; Perry et al., 1987, 1988; Farmer et al., 1989). In the pure shear model (e.g. Eaton, 1982; Fig. 1a), the entire lithospheric column deforms uniformly with the upper crust, and thus the location and magnitude of upper crustal extension corresponds to the amount and location of thinning of the underlying lithospheric mantle. In the simple shear model (e.g. Wer-

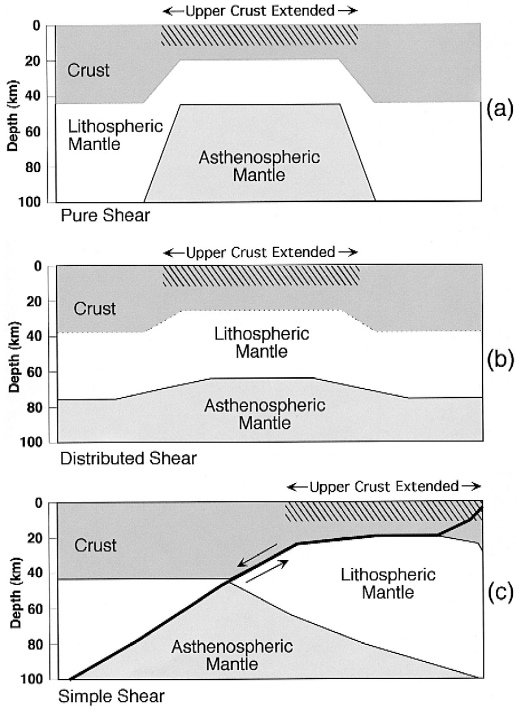

Fig. 1. Three models for the relationship between upper crustal extension and overall lithospheric thinning. (a) Pure shear model: Crust and mantle stretch and thin uniformly at all depths. (b) Distributed shear model: Thinning of the lithospheric mantle is distributed over an area larger than that of upper crustal stretching so that the maximum lithospheric thinning is less than in the pure shear model. (c) Simple shear model: Region of maximum lithospheric thinning is displaced laterally from the region of maximum upper crustal extension.

nicke, 1985; Fig. 1c) stress is transmitted through the lithosphere along discrete zones of shear, and the locus of maximum lithospheric thinning is displaced laterally from the zone of upper crustal deformation. Other models call for zones of lateral flow in rheologically weak areas of the lower crust and upper mantle (e.g. Wdowinski and Axen, 1992; Block and Royden, 1990; Wernicke, 1990) and predict that lithospheric thinning is distributed over areas larger than those affected by upper crustal deformation (Fig. 1b), or that lithospheric attenuation is averaged over distances of hundreds of kilometers (eg. Gans, 1987). The magnitude of thinning predicted by the lithospheric flow models depends on the area over which flow takes place. If the lithospheric thinning is distributed over a larger area than that affected by upper crustal extension, then the overall thinning of the lithosphere will be smaller than that corresponding to the upper crustal extension factors.

2. Isotopic stratigraphy of the lithosphere

A key assumption of the approach used here is that the continental lithosphere is markedly different in trace element composition and isotopic composition from the underlying asthenosphere. The model for this mantle stratigraphy is depicted schematically in Fig. 2 and supported by data from the study area discussed later in the paper. The model is based on the observation that continental basalts differ chemically and isotopically from mid-ocean ridge and ocean island basalts (Perry et al., 1987, 1988; Farmer et al., 1989; Daley and DePaolo, 1992; Bradshaw et al., 1993; Feuerbach et al., 1993; Rogers et al., 1995; Beard and Johnson, 1997). The special isotopic character of continental basalts is attributed to the continental lithospheric mantle. The origin of these differences in chemical and isotopic composition is controversial, but is generally attributed to addition of material enriched in incompatible elements to the lithospheric mantle at some time in the past. With time, and isolation of the lithospheric mantle from large scale mantle convection, radioactive decay of Rb and Sm (Lu, U, Th) gives rise to isotopic ratios of Sr and Nd (and Hf, Pb, etc.) in the lithosphere that are distinct from those of the asthenosphere. The trace element enrichment patterns attributed to the lithospheric mantle are similar to those of island arc volcanic rocks, and this observation has led to the hypothesis that the chemical ‘‘enrichment’’ of the lithospheric mantle occurs above subduction zones (e.g. Ormerod et al., 1988). Beard and Glazner (1995) challenge the subduction zone model with evidence from xenoliths, and argue convincingly that the age of the lithosphere beneath the Eastern Sierra Nevada region is not compatible with the subduction zone mechanism.

3. Depth of origin of basalts

Common basalt magma types generally have olivine, orthopyroxene and clinopyroxene as liquidus

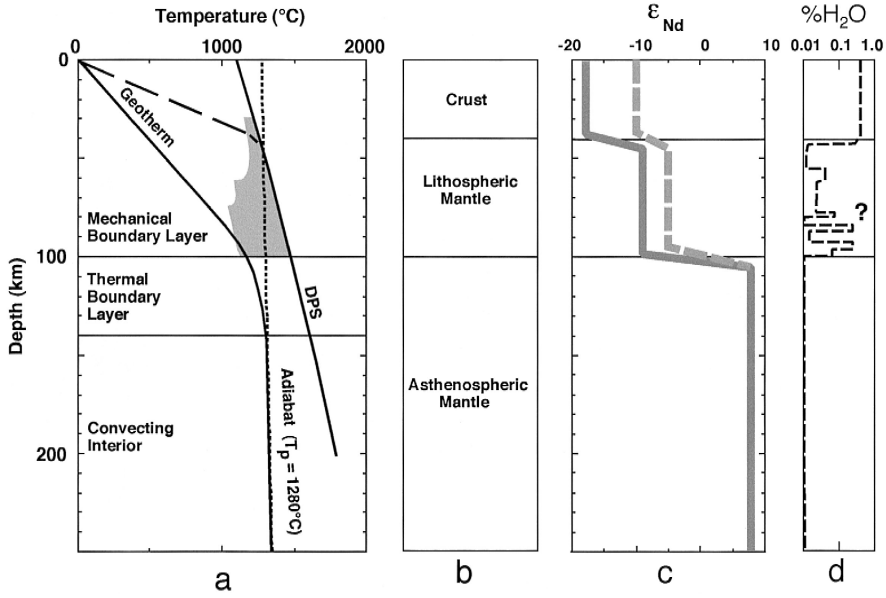

Fig. 2. Lithospheric stratigraphy inferred for the southwest Basin and Range. (a) Model profile of temperature in the lithosphere and upper asthenospheric mantle, adapted from McKenzie and Bickle (1988). DPS is the dry peridotite solidus. Solid curve is a stable geotherm corresponding to a 100-km-thick chemical lithosphere. Dotted line is an adiabat; long dashed line is an approximate geotherm after the lithosphere has been rapidly thinned to 40-km thickness. Shaded region is the extended melting region for H_2O-bearing peridotite. (b) Terminology used in this paper. (c) Inferred profile of ε_{Nd} in the crust and lithosphere of the Great Basin. The crustal values of $\varepsilon_{Nd} = -10$ and -18 correspond to the average values for crustal rocks from the 2.0–2.3 and 1.7–1.9 Ga basement provinces as estimated by Farmer and DePaolo (1983) and Bennett and DePaolo (1987). The values of ε_{Nd} for the lithospheric mantle are inferred from the data presented here in Table 1 and Fig. 9. Solid shaded line corresponds to regions of ca. 2 Ga crustal rocks; dashed shaded line corresponds to the eastern Sierra Nevada region. (d) Schematic distribution of H_2O, showing inferred regions of hydrous mantle in the lithosphere. To account for the small volume of volcanism during extension, only a small fraction the lithosphere needs to be hydrated.

phases at pressures of about 1.2 to about 3 GPa (Green, 1971), which corresponds to depths of 40 to 100 km. Since typical continental lithosphere extends to about 100-km depth, and the crust is about 40 km thick, the depth range of origin of most basalts corresponds to the depth range of typical continental lithosphere prior to extension. During extension, if the β factor (β = extended length/original length) reaches 2.5 or more, which is true for the Basin and Range Miocene extension, the lithosphere might be expected to thin from 100 to 40 km or less. Hence, prior to extension it would be expected that any basaltic magmatism would result from melting of the lithosphere. As extension proceeds, the depth range for basalt production should be occupied by asthenospheric mantle material that has moved upward to replace the thinning lithosphere; hence during and after extension, it would be expected that basaltic magma would result from melting either the lithosphere or the asthenosphere.

By considering the major element chemical composition of basalt lava, it is possible to place some further constraints on the depth of origin. This is a fundamental problem in igneous petrology, and there are still substantial uncertainties in determining, and even in defining, the depth of origin of particular magmas. Most magmatism outside of subduction zones is believed to originate by adiabatic upwelling of mantle material (e.g. McKenzie and Bickle, 1988), which can occur due to lithospheric extension or in mantle plumes (Watson and McKenzie, 1991). In adiabatic upwelling melting begins at a depth corresponding to the point where the upwelling mantle material has a temperature equal to that of its solidus. Melting continues to shallower depth as long as the upwelling is close to adiabatic, and is expected to

stop at a depth somewhat greater than that of the base of the lithosphere. The depth of melting is therefore actually a *depth range* of melting. The degree of melting is roughly proportional to the length of the depth range of melting, except at relatively shallow depth (Asimow et al, 1997). For mantle upwelling beneath lithosphere that is thicker than 40 km, melting is not expected to occur unless the mantle contains water or has an anomalous high temperature (McKenzie and Bickle, 1988; Arndt and Christensen, 1992). The anomalous high temperature of mantle plumes accounts for the melting that occurs at places like Hawaii where the lithosphere is 70 km thick (Watson and McKenzie, 1991). For anomalous hot mantle, or in the case of mid-ocean ridges where upwelling continues to very shallow depth, the depth range of melting can be quite large — up to 100 km. For the southern Basin and Range extension in the Miocene, there is no evidence of hot mantle (Bradshaw et al., 1993; Dodson et al., 1998) and the upwelling velocity is small (about 1 cm/year). Consequently, the depth range of melting is likely to be less than 10 km, and it is possible to consider the midpoint or top of this depth range as a reasonably well-defined ''depth of origin'' of the magma.

Depth of origin of basalts has an effect on the FeO, MgO, and SiO_2 contents of magma (Langmuir et al., 1992; Kushiro, 1996) and on the degree of silica undersaturation of the magmas (Takahashi and Kushiro, 1983; Green, 1971; Kushiro, 1996). A summary of the data of Kushiro (1996) which give a relatively complete picture for a specific mantle composition is shown as Fig. 3. Liquids in equilibrium with fertile mantle peridotite at pressures less than 10 kbar have normative hypersthene regardless of melt fraction. At 15 kbar and above, the liquids are nepheline normative for melt fractions smaller than about 10%, but hypersthene normative for larger melt fractions. For melt fractions in the 0% to 10% range, which apply to the magmatism associated with southwest Basin and Range extension, the crossover pressure is between 10 and 15 kbar, corresponding to a depth of about 35 to 45 km. This depth range would increase by about 5 to 10 km if the amount of K_2O in the peridotite starting material were decreased by half. In general, small degrees of partial melting and high pressures produce magmas with more normative nepheline, while larger degrees

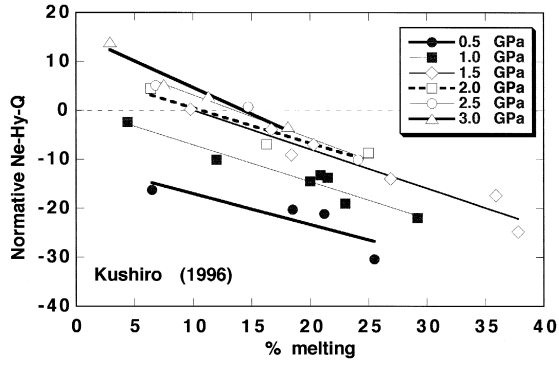

Fig. 3. Normative nepheline (Ne) vs. percent melting for the melting experiments of peridotite PHN1611 by Kushiro (1996). The vertical axis is normative Ne minus normative hypersthene (Hy) minus normative quartz (Q). At pressure below 2 GPa, there is strong pressure dependence on Ne–Hy–Q. At pressures of 2–3 GPa, there is much less pressure dependence. At melt fractions of 0% to 10%, the transition between Ne normative, and Hy + Q normative liquids occurs at a pressure of 1 to 1.5 GPa (corresponding to a depth of about 35–45 km under continents). With addition of 1% to 3% H_2O, or for a less K_2O-rich peridotite, these curves are expected to shift downward, increasing the transition depth for SiO_2 saturation by about 10 km.

of melting at lower pressures produce magma with normative hypersthene and quartz. Magmas classified as alkali basalt, with normative Ne contents between 0% and 10%, correspond to melt fractions of a few to 10%, and pressures above about 12–15 kbar. Nephelinites and melilitites, which typically have normative nepheline contents substantially greater than 10% (cf. Carmichael et al., 1973), presumably form only at pressures greater than about 25 kbar, and at melt fractions less than a few percent (Green, 1971).

The inferred depth at which magma with a particular value of normative Ne could have equilibrated with a peridotite source material varies with the water content of the magma and the potassium content of the magma source. Since normative composition does not take account of water content (most lavas degas almost completely upon eruption), the effect of water must be taken into account separately. In comparison to a dry magma, the same magma with 2.5% dissolved H_2O might form at a pressure up to 4 kbar higher, or a depth about 12 km greater (DePaolo, 1979). The Kushiro (1996) data suggest that for dry magmas the crossover depth of origin

should be at about 40 km. The actual depth of this crossover could be greater (due to the presence of water and the effects of olivine fractionation), but not shallower. Considering that many if not all lavas undergo some loss of olivine by fractional crystallization, and that they have water contents of 1% to 3%, the crossover depth may be closer to 50 km. If the magma source is poorer in potassium and sodium than the peridotite used by Kushiro (1996), the tholeiitic-to-alkaline transition would also occur at greater depth, so the crossover depth could potentially be as great as 60 km. Considering all of the possible effects, it is likely that a depth of 50 ± 10 km for the alkaline–tholeiitic transition is a reasonable estimate and uncertainty, assuming that the mantle has a normal potential temperature, and the melt fractions achieved are smaller than several percent (McKenzie and Bickle, 1988).

4. Effects of crustal contamination

Lava erupted through continental lithosphere can be contaminated with relatively high-SiO_2 rock material en route to the surface. The addition of high-SiO_2 material to a magma decreases the normative Ne content (or increases the normative Hy content) so that the derived lava would be inferred to have originated at a shallower depth. The extent of crustal contamination in the basalts considered here is discussed further in conjunction with the data analysis below. For similar rocks from the same area and of the same age, it was concluded that the amount of contamination was typically non-zero, but substantially less than about 10% by mass (Perry et al, 1987; Glazner and Farmer, 1992; Beard and Johnson, 1997; Beard and Glazner, 1998). This amount of contamination, depending on the SiO_2 content of the contaminant (and also the alkali content), would typically decrease normative Ne by up to 5%. The primary effect is to cause underestimation of the depth of origin by up to several kilometers.

As discussed further below, crustal contamination also causes shifts in isotopic composition, but these are small relative to the large contrast in values inferred for the lithosphere vs. the asthenosphere. For example, Glazner and Farmer estimated that lavas from the Cima volcanic field were shifted by 2 to 3 units of ε_{Nd} by crustal contamination. Similar estimates were obtained by Perry et al. (1987), Beard and Johnson (1997) and Beard and Glazner (1998). The contrast in ε_{Nd} between the lithosphere and asthenosphere is 13 to 18 units of ε_{Nd}, so the crustal contamination effects should be minor and not significantly affect the interpretations.

5. Expected isotopic shifts during extension

Fig. 4 shows how the lithosphere–asthenosphere boundary should approach the earth's surface during extension, assuming that the lithosphere thinning is by pure or distributed shear. The time scale and extent of thinning is taken from the model of Wernicke and Snow (1998) for the Lake Mead Extensional Area (LMEA), where extension of a factor of about 3 to 4 took place, mostly between 16 and 10 Ma. For an initial lithosphere thickness of 100 km, the boundary begins well below the transition depth for tholeiitic vs. alkaline basalt generation. As extension proceeds the boundary becomes shallower and eventually passes into the depth range where tholeiitic basalt can be generated. If alkali basalt is produced before, during, and after extension, the isotopic compositions of the basalts should vary with age. Those erupted before extension should derive from the lithosphere and have lithospheric isotopic signatures (low ε_{Nd} value), assuming that the starting thickness of the lithosphere is greater than 80 km. Those erupted after the lithosphere has thinned to less than 50 ± 10 km will have either asthenospheric isotopic signatures, or possibly isotopic signatures that are mixtures of asthenospheric and lithospheric. The structure of the transition in isotopic composition with time depends on the sharpness of the lithosphere–asthenosphere boundary, the amount and time-history of extension, and the relationship between lithospheric thinning and extension as diagrammed in Fig. 1.

An important and unresolved question is why basalt is generated from the lithosphere. Under ''normal'' conditions, the solidus of dry peridotite is not intersected by the geotherm under continents (Fig. 2a). Consequently, there should be no melting unless the lithosphere is thinned to a thickness of about 40 km, or unless the temperature of the mantle is sub-

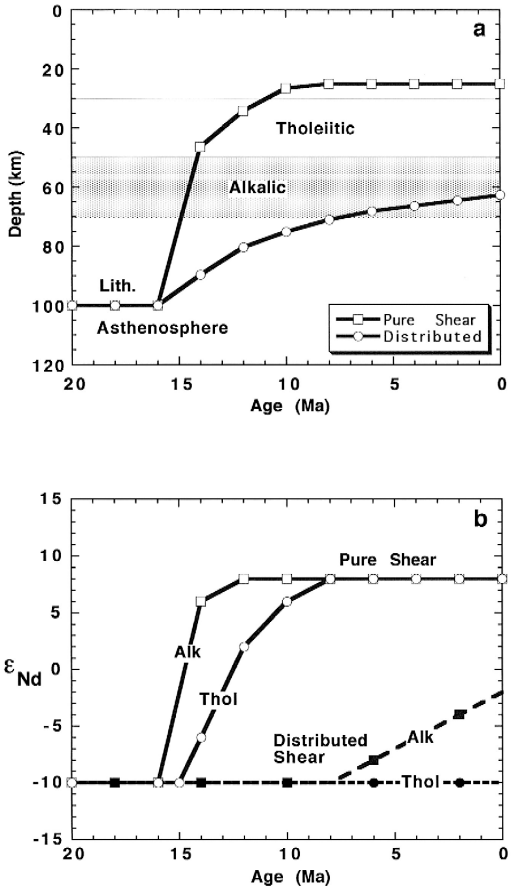

Fig. 4. (a) Model predictions for depth to the lithosphere–asthenosphere boundary vs. age for the Lake Mead extensional area (see Fig. 6). The curve labeled ''pure shear'' is based on the amount of extension vs. age for the Lake Mead area. The curve labeled ''distributed shear'' corresponds to the average thinning for the entire extended area between the Colorado Plateau and the Sierra Nevada at about 37°N Latitude (Wernicke and Snow, 1998). The inferred depth range of the source regions of tholeiitic basalt (30–50 km) and alkali basalt (50–70 km) are also shown. (b) Expected changes in the ε_{Nd} of alkalic and tholeiitic basalts during extension for the pure shear and distributed shear models. The assumed lithospheric isotopic structure is the solid shaded line in Fig. 2d.

stantially higher than 1280°C (McKenzie and Bickle, 1988; Arndt and Christensen, 1992). In the southern Basin and Range, there is no indication of a mantle plume that would provide high temperature (Bradshaw et al., 1993; Dodson et al., 1998), so no melt is expected to be generated during extension. To first order this statement is correct for the area under consideration, because the amount of magma generated is extremely small. The total average thickness of melt generated during extension in the Southwest Basin and Range province is 0.0001 to 0.01 km (corresponding to 10–1000 km^3 of lava erupted over an area of 100,000 km^2). The amount is unevenly distributed; it is less in the interior part of the region under consideration and higher (but still low) on the eastern and western edges. The values of 0.0001 to 0.01 km can be compared to the 7-km thickness of melt generated at mid-ocean ridges, about 10^3 to 10^5 times more than in the southwest Basin and Range province. Therefore, the magma erupted during extension is a second-order effect, and is presumably generated from heterogeneities in the lithosphere that can melt at low temperature either because of the presence of water or because they are relatively pyroxene-rich (Harry and Leeman, 1995). The effect of water on promoting lithospheric melting has been discussed previously, albeit in a different context, by Gallagher and Hawkesworth (1992). In a later section, we discuss the effect of water in the lithosphere on the estimates of depth of origin of lithosphere-derived magmas.

6. Tectonic and magmatic history

The lithospheric mantle beneath the southwestern U.S. is divisible into three major provinces based on the geochemistry of the erupted basalts. These provinces bear some resemblance to the provinces that have been delineated in the Precambrian basement (Farmer and DePaolo, 1983; Bennett and DePaolo, 1987; Farmer, 1988), but also reflect the complex Phanerozoic geologic history of the region (Stewart, 1975; Nelson, 1981; Dickinson, 1981; Smith, 1981; Atwater, 1970). Most of the continental crust of the Southwest Basin and Range lies within the 2.0–2.3 Ga model age ''Province 2'' of Bennett and DePaolo (1987) (Fig. 5). The mantle lithosphere can be divided into three major provinces. The eastern province coincides with the limits of the Colorado Plateau. The western province includes the region immediately east of the Sierra Nevada (shaded region in Fig. 5) plus the Mojave Desert and the region north of the limit of Precambrian basement in western Nevada. The central province is the region between. The documentation of the difference be-

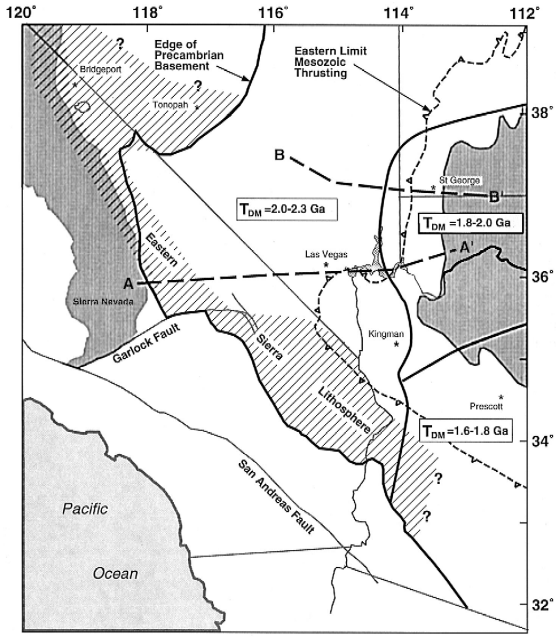

Fig. 5. Map of the southwestern U.S. showing the distribution of crustal Nd model age provinces, the western limit of Precambrian basement, and the inferred distribution of mantle lithosphere isotopic provinces. The western edge of the Precambrian basement and the eastern limit of Mesozoic thrusting are from the Tectonic Map of North America (Bayer, 1983). Nd model age crustal provinces are modified after Bennett and DePaolo (1987), T_{DM} ages in boxes refer to these provinces. The ruled area is the Eastern Sierra mantle lithosphere province, defined on the basis of data presented here. Approximate cross-section line for Figs. 12 and 13 are shown as line A–A′. The cross-section line for Fig. 14 is labelled B–B′.

tween the central and western provinces is given below. The eastern province is not involved in the extension significantly, but differs from the other two provinces mainly by being more heterogeneous (Kempton et al., 1991; Daley, 1992).

Most of the Basin and Range underwent several episodes of upper crustal extension and volcanism during the Cenozoic (Stewart, 1975; Atwater, 1970; Glazner and Bartley, 1984; Dickinson and Snyder, 1979; Sonder et al., 1987; Wernicke et al., 1987; Fitton et al., 1991; Faulds et al., 1990). The southwestern part of the Basin and Range, the area from ca. 37°N Latitude to the Garlock Fault on the west and to west central Arizona on the east, and from the relatively stable Colorado Plateau to the Sierra Nevada, has undergone only one main episode of upper crustal deformation and mafic magmatism beginning at about 16 Ma. This region, sometimes called the ''amagmatic corridor'', also did not experience the widespread and voluminous silicic volcanism that accompanied the Eocene to Miocene extension (Farmer et al., 1989; Glazner and Bartley, 1984). The volcanic activity associated with the post-16 Ma extension is mainly basaltic, and generally concentrated at the margins of the extended area (Luedke and Smith, 1981). In the Mojave Desert area, the extension was earlier, only one main period of extension took place, and silicic volcanism gave way to basaltic (or ''bimodal'') volcanism at approximately the time extension ceased at about 18 Ma (Armstrong and Higgins, 1973).

Five major extensional areas are considered here (Fig. 6). Three of these occur in an east–west transect between about 36° and 37°N Latitude. Las Vegas, Lake Mead and surrounding areas are included in the LMEA, in which deformation began at about 16 Ma (Anderson et al., 1972; Darvall et al., 1991; Fitzgerald et al., 1991) and progressed westward, continuing until about 10 Ma. In the Death Valley Extensional Area (DVEA) deformation occurred mainly between 10 and 4 Ma (Wernicke et al., 1988;

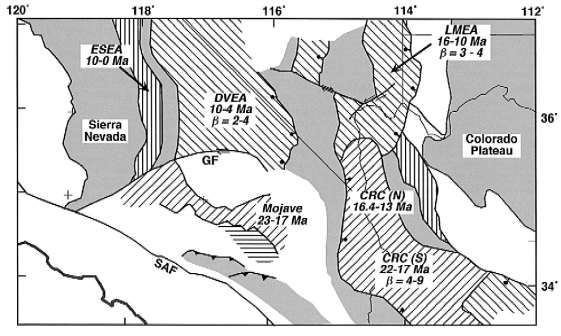

Fig. 6. Extensional domains of the SW Basin and Range after Spencer and Reynolds (1986): LMEA (Lake Mead Extensional Area), DVEA (Death Valley Extended Area), ESEA (Eastern Sierra Extended Area), CRC (Colorado River Extensional Corridor), Mojave extensional area. Ages given correspond to the period of major extension. Shaded areas are regions of relatively little deformation, lined patterns are regions with extensive upper crustal deformation; NE–SW lined areas have dominantly W dipping Tertiary strata, NW–SE lined areas have dominantly E dipping Tertiary strata, E–W and N–S lined areas do not have clearly dominant regional dips (Stewart, 1980a,b). Breakaway faults shown by solid lines with knobs in the direction of hanging wall transport.

Snow and Wernicke, 1989; Wernicke and Snow, 1998). The LMEA and DVEA are separated by a region that experienced relatively little Miocene deformation (Wernicke et al., 1988; Spencer and Reynolds, 1986). In the Eastern Sierra Extensional Area (ESEA) extension began at about 10 Ma, and continues to the present; the opening of the Panamint Valley having occurred within the past 4 Ma (Wernicke et al., 1988; Schweig, 1984). Both the Las Vegas and the Death Valley systems are characterized by west-directed low angle normal faulting, resulting in consistently east-dipping Tertiary strata across the region.

Extension in the Mojave Desert and western Arizona also occurred in two highly extended belts — the central Mojave and the Colorado River Corridor (CRC) — separated by an area of relatively little deformation in the eastern Mojave (Bartley and Glazner, 1991). In the central Mojave, the main period of extension was from 23 to 20 Ma, followed by relatively minor extension between 20 and 17 Ma (Dokka, 1986; 1989). Two parts of the Mojave terrain have Tertiary strata dipping in opposite directions, implying opposite-sense motion on low angle normal faults (Dokka, 1989). Extension in the southern CRC occurred from 23 to 25 Ma (Foster et al., 1991; Spencer and Reynolds, 1991). The age of extension decreases northward in the CRC from 22–17 Ma in the Whipple Mountains to 16.4–13 Ma near a structural accommodation zone that separates east-directed normal faulting in the CRC (Shackleford, 1980; Spencer and Reynolds, 1986; Howard and John, 1987) from west-directed normal faulting in the Las Vegas area (Faulds et al., 1990, 1992).

Wernicke et al. (1988) and Snow and Wernicke (1989) estimated net extension across the area from the Colorado Plateau to the Sierra Nevada by measuring relative motion vectors between three sets of structural and stratigraphic markers. Across a transect currently about 360 km wide, the total extension is estimated to be 247 ± 56 km in a direction $S73^\circ \pm 12^\circ E$ (Wernicke et al., 1988; Snow and Wernicke, 1989; Wernicke and Snow, 1998). On the basis of these data, β for the transect is approximately 3, with lower and upper limits of 2 and 6, respectively. The most intense stretching occurred at the margins of the transect in the southern part of the Death Valley region to the west ($\beta \approx 4$) and the Las Vegas area to the east ($\beta = 3–4$; Wernicke et al., 1988). For the CRC-Mojave region, Spencer and Reynolds (1986, 1991) estimate that a region originally 10 to 20 km wide was extended by 86 ± 13 km in a northeasterly direction (Spencer and Reynolds, 1991). These figures imply an extension factor of $\beta = 4–9$. Extension on one of the regional detachment faults dies out to the north (Spencer and Reynolds, 1991), consistent with the observation that the degree of extension decreases from the southern CRC to the Accommodation Zone (Faulds et al., 1992).

At present, the crust is approximately 30 km thick in the Las Vegas-Death Valley area, and about 25-km thick in the Mojave Desert and the Colorado River Trough (Pakiser, 1989; Allenby and Schnetzler, 1983; De Voogd et al., 1988). To the east and west of the Basin and Range, crustal thicknesses increase rapidly to ca. 45 km in the Colorado Plateau area and 50 km in the Sierra Nevada (Pakiser, 1989; Allenby and Schnetzler, 1983). The rheologic lithosphere defined by seismic velocity structure is about 50–65 km thick near Las Vegas, and thickens to 80–100 km beneath the Colorado Plateau (Smith et al., 1989; Zandt et al., 1995). The pre-extension crustal and lithospheric thickness in the eastern Basin and Range were probably similar to that of the Colorado Plateau. Thickening of the upper crust to the west of Las Vegas by Mesozoic thrusting makes it more difficult to estimate the initial crustal and lithospheric thickness in the western Basin and Range.

7. Samples and analytical procedures

Mafic lava samples were collected for Nd and Sr isotopic analysis and for major and trace element analysis (Table 1). Radiometrically dated flows were sampled where possible, but for flows where radiometric dates were not published, whole-rock K–Ar ages were determined (Table 2). Sample locations, ages and descriptions as well as radiometric age references are tabulated in the Appendix, and locations of all samples used are shown in Fig. 7. Sample locations corresponding to published isotopic and chemical analyses from other sources are also shown in Fig. 7.

Samples were broken into ca. 10 cm or smaller pieces in the field, and those with visible alteration

Table 1
Isotopic and chemical data and ages for basaltic lava samples

	Age (Ma)	ε^{a}_{Nd}	$^{87}Sr/^{86}Sr^{a}$	SiO_2	TiO_2	FeO^T	MgO	Mg#[b]	Q	Ne	Hy	Ol	Ni	Rb*	Sr*	Zr	Ba	La	Ce	Nd*	Sm*	La/Nb	Ba/Nb	Zr/Y
Lake Mead Extensional Area																								
TPV-2	15.2	−9.4	0.70878	55.7	1.30	6.12	3.91	0.57	2.9		12.5		60	89.6	1031	311	1524	84	152	70.3	10.7	3.77	68.1	11.9
TPV-2 CPX[c]		−9.1	0.70871																					
TPV-8	17	−11.1	0.70965	55.1	1.17	5.59	5.65	0.68		1.5		10.3	135	83.6	1254	365	1761	96	180	89.6	12.9	6.55	119.1	15.8
TPV-8 CPX[c]		−9.8	0.70926																					
TDM-2	13	−6.1	0.70720	53.5	1.52	7.65	6.65	0.65			1.2	11.4	109	39.6	588	232	683	51	92	40.7	6.9	1.88	24.9	8.4
TDM-5	13	−5.3	0.70694	52.0	1.62	7.93	6.99	0.65		0.6		13.5	129	37.6	615	253	602	45	93	41.3	7.4	1.61	21.2	8.6
TDM-9	13	−7.4	0.70667	55.3	1.37	7.02	5.15	0.61			11.5	1.7	55	50.4	748	234	807	53	98	43.1	7.2	2.48	37.2	8.6
714-35	12.5	−6.1	0.70705	45.0	2.90	9.76	6.98	0.60		9.0		10.0	73	25.1	1215	219	1784	83	147	72.6	11.4	2.43	51.6	8.0
714-35 CPX[c]		−7.9	0.70700																					
TMV-1	9.5	−10.1	0.70753	56.5	1.14	8.29	4.24	0.52	5.4		15.1		69	44.1	397	153	726	30	63	25.1	5.4	2.35	56.5	5.9
TMF-5	10.5	−8.4	0.70739	49.9	1.28	11.51	7.70	0.58			11.5	10.0	164	11.9	246	109	231	15	34	14.2	3.3	4.05	60.6	4.5
TMF-9	10.5	−7.9	0.70746	49.4	1.25	11.57	7.12	0.56			3.7	14.2	173	10.9	267	107	278	16	33	15.7	3.6	5.88	99.2	4.5
TMF-2	4.9	−0.2	0.70519	47.5	1.89	9.70	5.77	0.56	8.1		12.8		16	19.4	665	169	814	49	80	36.8	6.4	1.38	22.5	6.3
TID-1	4.6	5.4	0.70471	45.8	2.93	8.96	4.07	0.49		3.3		7.6	97	38.0	1139	262	1012	45	93	39.9	7.2	0.62	13.9	9.8
TID-1 Hb[c]	4.6	6.4	0.70 293																					
91-23	9.4	−1.3	0.70493	48.1	1.67	10.89	7.74	0.60		4.5		16.2	190	18.8	446	163	293	22	49	24.0	4.9	0.94	12.2	6.0
91-24	5.72	1.2	0.70461	48.7	1.55	8.21	7.00	0.64		2.6		14.2	62	27.1	707	184	762	44	69	28.3	5.0	0.84	14.4	7.8
91-25	9.4	−1.6	0.70510	47.7	1.59	10.98	8.35	0.62		3.3		18.3	207	18.1	409	155	300	23	43	23.3	4.6	1.00	13.0	5.9
91-26	5.1	−0.5	0.70490	49.2	1.38	11.48	7.69	0.59		4.0		16.7	131	6.5	335	106	206	9	28	14.4	3.5	0.74	15.7	4.6
91-27	4	4.3	0.70366	50.1	1.98	11.16	7.66	0.59		3.8		15.5	196	14.1	429	161	265	20	46	20.9	4.4	0.82	10.8	7.0
91-29	3	2.7	0.70386	50.7	2.09	11.14	6.77	0.56		3.3		13.4	56	13.2	437	168	358	23	44	23.0	4.9	0.90	13.7	6.3
91-30	3	7.0	0.70325	47.6	2.39	11.43	6.35	0.54		12.6		12.2	116	25.5	755	255	401	32	64	34.0	7.0	0.65	8.0	11.4
91-31	3	5.9	0.70338	49.6	2.09	10.94	7.72	0.60		10.2		15.6	173	23.5	645	220	386	25	59	28.6	5.9	0.64	9.6	9.0
91-32	3	6.0	0.70342	49.4	2.15	11.25	7.49	0.58		8.4		15.4	154	22.2	606	209	349	26	47	27.7	5.8	0.70	9.2	8.8
91-33	4.3	−0.4	0.70456	49.7	1.44	11.18	7.13	0.57			2.1	14.7	103	9.6	335	110	248	14	28	16.1	3.6	1.08	19.0	4.6
91-34	4.3	−0.3	0.70453	49.4	1.49	11.10	6.18	0.54			4.3	11.2	68	9.0	356	118	302	16	30	17.1	3.9	1.17	20.9	4.9
Mojave Desert area–Piute Mountains																								
91-5d	19.9	−3.8	0.70750	57.5	1.06	7.26	5.17	0.60	8.5		17.2		58	140.0	390	162	572	26	50	23.9	4.6	2.45	53.6	7.2
91-9	14	−5.9	0.70638	55.3	1.23	6.34	4.09	0.58	1.8		12.4		26	51.4	717	233	896	52	97	40.9	6.7	2.19	37.5	9.0
91-12	14	−5.3	0.70596	53.6	1.15	6.80	4.81	0.60	1.3		14.1		35	38.2	819	200	868	50	91	41.9	6.7	2.36	40.7	8.4
Colorado River Corridor																								
91-14	19.9	−8.5	0.70913	55.9	1.25	6.20	4.06	0.58	0.5		10.9		77	165.1	1119	248	1175	70	143	64.4	9.8	3.41	56.9	10.1
91-16	14.6	−8.1	0.70840	53.2	1.32	7.28	5.25	0.60			6.6	5.4	76	36.2	776	216	828	45	92	42.6	7.1	2.27	41.3	8.0
91-49	9.2	−7.3	0.70732	56.9	1.02	7.42	5.07	0.59	4.0		15.6		78	53.4	320	172	544	29	58	25.9	5.0	1.80	33.7	6.7

91-51	7.5	3.7	0.70441	48.6	2.38	11.36	5.82	0.52		0.3		12.6	40	13.5	406	192	398	20	47	27.2	5.9	0.68	13.1	6.3
91-52	11.3	−6.3	0.70691	52.0	1.38	8.50	5.38	0.57			15.8	0.8	52	23.4	535	177	577	35	68	32.2	5.6	2.39	39.5	6.1
91-53	7.5	6.1	0.70338	47.7	2.11	9.94	6.94	0.60		5.2		14.4	75	21.8	567	209	241	26	56	28.5	5.8	0.70	6.4	8.3
91-19	19	−9.3	0.70916	58.9	1.10	5.63	5.01	0.65	7.4		14.4		146	52.6	1027	219	1292	50	112	52.6	8.1	3.44	87.6	11.2
91-20	19	−9.4	0.70955	58.8	1.16	5.62	3.70	0.58	6.1		11.5		69	102.0	889	295	1082	77	152	70.0	10.2	3.54	49.6	11.2
Death Valley Area																								
91-41	4	−2.9	0.70635	54.6	1.50	7.92	4.71	0.56	1.4		14.6		54	43.8	610	215	775	32	71	35.9	6.4	1.73	42.0	8.0
91-42	4	−8.0	0.70776	57.4	1.24	6.28	3.92	0.57	6.9		11.2		26	53.8	679	226	902	53	100	44.0	7.0	2.64	45.0	9.6
91-43	1.5	−9.3	0.70711	53.6	1.53	8.18	3.70	0.49	1.8		14.4		23	38.6	1041	307	1133	79	151	69.2	10.0	2.22	31.6	12.2
91-44	0.69	−9.5	0.70697	50.5	1.88	9.71	4.86	0.51			4.6	9.7	37	29.0	1211	284	979	74	148	70.9	10.9	2.34	30.8	10.2
91-47	15	−6.2	0.70733	55.9	0.99	5.63	3.55	0.57	2.6		10.1		48	72.9	1247	260	1324	71	138	66.8	9.9	4.54	83.8	10.2
Nevada–California border area																								
91-54	0.5	−2.1	0.70589	47.7	1.85	9.09	7.28	0.63		9.1		14.3	113	43.6	968	185	971	34	73	40.1	7.0	1.21	34.2	7.2
91-55	6.4	−5.7	0.70672	47.5	1.10	7.56	6.78	0.65		5.6		13.6	90	32.2	1227	130	981	30	67	37.6	6.2	2.96	96.5	6.6
91-56	3.5	−4.5	0.70617	52.7	1.18	6.20	6.64	0.69			11.4	4.5	84	70.7	866	238	1527	28	51	28.9	5.3	1.94	105.3	10.6
91-57	5.8	−3.5	0.70602	53.9	1.34	7.08	4.81	0.59			6.0	8.3	73	67.4	1019	232	1543	50	100	49.0	7.9	2.25	69.5	8.7
91-58	5.5	−0.9	0.70515	53.7	1.07	7.41	5.73	0.62			13.4	2.0	32	24.7	905	115	763	20	43	21.9	4.3	4.71	177.5	6.2
91-59	10.8	−2.8	0.70566	59.9	0.72	5.05	3.12	0.57	9.5		11.0		31	74.0	653	150	1086	24	49	21.6	4.0	4.06	182.7	8.3
91-60	9.3	−3.5	0.70576	53.7	1.22	6.47	2.50	0.45	0.8		10.1		6	121.5	840	194	1505	34	76	38.8	7.2	3.75	163.2	8.1
91-61	9.2	−2.5	0.70590	54.1	1.20	6.62	3.28	0.51	2.0		9.7		31	51.7	840	139	992	19	50	28.1	5.5	2.19	112.7	6.5
91-62	0.124	−1.3	0.70590	48.9	1.50	8.64	6.65	0.62		6.7		13.0	91	11.8	860	144	519	24	53	26.9	5.1	2.24	47.7	6.2
Eastern Sierra Extensional Area																								
91-63	0.5	−2.1	0.70587	52.2	1.32	7.25	6.63	0.66		2.3		12.4	89	24.9	638	170	689	20	52	25.8	5.0	2.67	88.4	6.8
91-64	0.5	−4.8	0.70647	51.9	1.34	6.87	6.35	0.66		1.6		12.4	106	33.7	823	184	946	34	55	31.4	5.7	2.71	74.1	8.3
ECDP	4.9	−3.5	0.70554	51.3	1.16	7.01	6.52	0.66		9.0		8.1	44	15.6	830	122	572	16	41	21.0	4.2	2.15	75.8	5.5
91-65	5.7	−5.7	0.70626	50.9	1.36	7.91	5.05	0.57			5.8	7.4	24	26.3	870	162	720	28	67	30.6	5.3	2.02	52.0	7.3
91-66	6.3	3.7	0.70487	48.6	1.83	8.88	6.81	0.62		6.5		12.1	82	15.6	820	173	523	23	57	29.6	5.8	1.38	31.6	6.3
91-67	3.56	−0.1	0.70543	51.5	1.43	7.72	5.88	0.62		3.3		10.8	41	14.0	834	163	546	18	37	24.7	5.0	3.03	91.0	6.6
91-68	0.14	4.0	0.70445	48.4	2.06	9.18	6.00	0.58		4.1		12.5	41	14.3	746	171	434	24	51	29.8	5.8	1.19	21.0	6.4
91-69	0.1	−0.3	0.70547	49.8	1.65	8.33	5.74	0.59		2.4		11.6	42	18.1	971	152	733	26	62	34.4	6.1	2.08	58.5	6.2
91-70	0.486	2.3	0.70468	52.0	1.72	8.12	5.74	0.60		0.7		12.0	47	21.3	550	176	664	27	62	23.4	4.5	1.45	35.1	7.6

Concentrations were determined using X-ray flourescence except for those with asterisks, which were determined using isotope dilution.

[a]The ε_{Nd} values are calculated relative to a modern CHUR value of 0.511836, corresponding to normalization using $^{142}Nd/^{146}Nd = 0.636151$. The $^{87}Sr/^{86}Sr$ measured for the NBS987 standard is 0.71029.

[b]The Mg number is calculated assuming that 85% of total Fe as FeO is divalent.

[c]For these samples, phenocrysts of clinopyroxe (CPX) or hornblende (Hb) were measured to check for alteration effects in the whole rock samples.

Table 2
Potassium–argon geochronology

Sample #	%K			^{40}K (ppm)	^{40*}Ar (10^{-4} ppm)				^{40*}Ar/^{40}Ar$_{Total}$				^{40*}Ar/^{40}K ($^{*}10^{-4}$)	Age (Ma)	±
	1	2	Average		1	2	3	Average	1	2	3	Average			
ECDP	1.002	0.985	0.994	1.185	3.47	3.30		3.38	0.320	0.228		0.274	2.86	4.9	0.3
91-9	1.995	2.019	2.007	2.394	19.75	19.28		19.52	0.606	0.617		0.612	8.15	14.0	0.5
91-12	1.547	1.490	1.519	1.812	14.81	14.77		14.79	0.520	0.537		0.528	8.16	14.0	0.5
91-26	0.643	0.649	0.646	0.771	2.39	2.20		2.30	0.255	0.234		0.244	2.98	5.1	0.3
91-33	0.711	0.705	0.708	0.845	1.98	2.27		2.13	0.220	0.229		0.224	2.52	4.3	0.3
91-40	0.952	0.957	0.955	1.139	5.96	5.96		5.96	0.353	0.411		0.382	5.23	9.0	0.4
91-55	1.638	1.654	1.646	1.964	7.28	7.42		7.35	0.413	0.248		0.330	3.74	6.4	0.3
91-56	3.049	3.084	3.067	3.658	7.41	7.55		7.48	0.338	0.351		0.344	2.04	3.5	0.2
91-57	2.752	2.731	2.742	3.271	11.32	10.94		11.13	0.447	0.598		0.522	3.40	5.8	0.2
91-65	1.433	1.472	1.453	1.733	5.89	5.70		5.80	0.185	0.418		0.113	3.34	5.7	0.3
91-66	0.971	0.993	0.982	1.172	4.31	4.32		4.32	0.329	0.404		0.366	3.68	6.3	0.4

K–Ar determinations by Krueger Enterprises, Geochron Laboratories division, Cambridge, MA.
All determinations done on whole-rock samples, $-80/+200$ mesh sieved fraction with mafic minerals with density >3.20 removed, and treated with dilute HF and HNO_3.

were discarded. After examination of thin sections, those samples that showed the smallest degree of alteration were selected for analysis. Each sample was crushed in a tungsten carbide-lined piston mortar and pestle. The sieved fraction between 3/8 and 18 mesh size was hand picked to remove fracture alteration and vesicle fillings and then pulverized in a tungsten carbide shatter box for 4 min. Where it was not feasible to remove all vesicle filling material, the hand-picked fraction was leached in 2.5 N acetic acid for 30 min and rinsed in distilled water in an ultrasonic bath. Nd and Sr isotopic compositions measured on leached and unleached fractions of these samples were within analytical error, indicating that vesicle fillings either had very low concentrations of Sr and Nd and/or had Nd and Sr isotopic compositions very similar to those of the host. In cases where the lava sample was substantially altered, phenocryst separates were also measured.

Nd and Sr isotopic compositions and concentrations of K, Rb, Sr, Sm, and Nd were measured on all samples at U.C. Berkeley in the Berkeley Center for Isotope Geochemistry. Splits of the pulverized sample or mineral separate (100–200 mg) were completely digested in HF and $HClO_4$, and an aliquot was spiked with a mixed K, Rb, Sr, Sm, and Nd tracer solution for isotope dilution measurements. Sr and Nd were separated from an unspiked 60–100 mg aliquot using ion exchange chromatography according to the procedure of DePaolo (1978). Total chemistry blanks for Sr and Nd were 320–480 pg Sr and 16–23 pg Nd.

The Nd and Sr isotopic ratios were measured using a VG Instruments Sector 54-E 8-collector mass spectrometer run in the dynamic mode. For Sr, approximately 100 ng was loaded in 1 μl of HNO_3 onto a bed of TaO slurry on a Rhenium ribbon filament. Analyses were done at a current of 4×10^{-11} A for the $^{88}Sr^{+}$ peak at a filament temperature of 1200–1400°C. At least 50 measurements of each isotope were done, with each peak integrated for 5 s in each measurement. Duplicate analyses of $^{87}Sr/^{86}Sr$ agreed to within 0.00003, and 24 analyses of the NBS-987 standard run during the same period gave $^{87}Sr/^{86}Sr = 0.710291 \pm 20$. Sr isotopic ratios are normalized to $^{86}Sr/^{88}Sr = 0.1194$. For Nd, 100 ng was loaded in 5% HNO_3 onto a Re ribbon filament. Oxygen was bled through a valve into the source chamber of the mass spectrometer to maintain a pressure of 1.0×10^{-6} Torr throughout the run. A minimum of 100 measurements was done, with an ion current of 0.35 to 1×10^{-11} A for the $^{146}Nd^{+}$ peak, and each Nd measurement was integrated for 5 s. In addition to the Nd isotopes, $^{141}Pr/^{144}Nd$ and $^{154}Sm/^{144}Nd$ were measured and corrections for interferences of these elements were done off-line

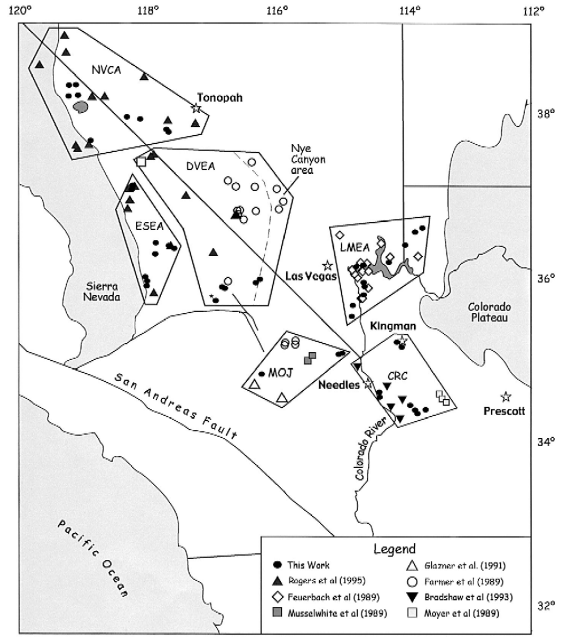

Fig. 7. Sample location map. Samples from this study (Table 1) are shown as solid black circles. Polygons enclose samples by geographic location: LMEA (Lake Mead Extensional Area), DVEA (Death Valley Extended Area), ESEA (Eastern Sierra Extended Area), CRC (Colorado River Extensional Corridor), (MOJ) Mojave extensional area, NVCA (Nevada–California border region). The dashed line within DVEA delineates the zone along the eastern edge including Nye Canyon that shows isotopic evidence of lithospheric thinning. The open square in DVEA is the location of the Deep Springs Valley lavas described by Beard and Glazner (1998), which have significantly lower ε_{Nd} values than other lavas in the southwestern U.S. The sample location with asterisk in the southwestern corner of DVEA is inferred to be in Eastern Sierra lithosphere (see Fig. 6).

(after the procedure of Wasserburg et al., 1981). $^{140}Ce/^{144}Nd$ was also monitored, and in all cases was indistinguishable from zero. Samples were re-separated and re-analyzed if the Sm or Pr correction was more than 0.3 ε units of the $^{143}Nd/^{144}Nd$ ratio. Duplicate analyses agreed to better than 0.5 ε units. The California Institute of Technology standard CIT-67 was measured over the same time period as $^{143}Nd/^{144}Nd = 0.511103 \pm 10$ ($n = 3$); and Nd standard BCR-1 was measured as $^{143}Nd/^{144}Nd = 0.511832 \pm 16$ ($n = 8$). Nd isotopic ratios were normalized to $^{146}Nd/^{142}Nd = 0.636151$, and corrected for oxygen isotopes assuming that $^{17}O/^{16}O = 0.000387$ and $^{18}O/^{16}O = 0.00211$. ε_{Nd} is calculated relative to $^{143}Nd/^{144}Nd_{(CHUR)} = 0.511836$:

$$\varepsilon_{Nd} = 10^4 \left[\frac{^{143}Nd/^{144}Nd_{sample}}{^{143}Nd/^{144}Nd_{Chur}} - 1 \right]$$

Major element oxide concentrations were measured by X-Ray Fluorescence Spectrometry at U.C. Berkeley using fused glass discs and natural rock standards. Trace element concentrations were also determined at UCB using pressed powder pellets and natural rock standards (Table 1).

Whole-rock K–Ar ages of 17 samples were determined (Table 2) by Geochron Laboratory (Kreuger Enterprises, Cambridge, MA). Samples were crushed to $-80/+200$ mesh and treated with HF and HNO_3 in an ultrasonic bath to remove devitrified glass and other alteration products. Non-potassic mafic minerals, which have the potential of carrying excess Ar, were removed by floating the samples in specific gravity 3.20 heavy liquid.

8. Results

The data obtained in this study are listed in Tables 1 and 2. Although full chemical analyses were determined, only the essential data are included in Table 1. In four cases, the lava samples were sufficiently altered that clinopyroxene or hornblende mineral separates were made and analyzed to check the isotopic compositions of Sr and Nd. The mineral analyses were used to represent the isotopic compositions of these samples. In two cases the clinopyroxene data do not exactly match the whole rock data. In one case clinopyroxene has a higher ε_{Nd} by about 1 unit, and in the other case it has a lower ε_{Nd} by about 1 unit. There are corresponding differences in $^{87}Sr/^{86}Sr$. However, in both cases the clinopyroxene is sufficiently close in isotopic composition that exchanging its values for the whole rock values does not affect the conclusions significantly. For sample TID-1, an alkalic dike sample, the hornblende $^{87}Sr/^{86}Sr$ value is considerably lower than the whole rock value, and more consistent with the ε_{Nd} value. The difference between the mineral and the whole rock values may be due to magmatic processes rather than post-emplacement alteration.

The Nd isotopic data for the lavas from the LMEA, CRC, and DVEA (Table 1; Fig. 7), plus data from the LMEA by Feuerbach et al.(1993) are plotted against SiO_2 content and Mg# in Fig. 8. The data indicate that crustal contamination cannot account for the major isotopic variations in the lavas, as noted previously by others (Perry et al, 1987; Glazner and Farmer, 1992; Beard and Johnson, 1997; Beard and Glazner, 1998). Virtually the entire range of ε_{Nd}, from +7 to −9, is covered by lavas with SiO_2 contents less than 50% (Fig. 8a) The samples with higher SiO_2, which are the Hy normative ones, extend the range of ε_{Nd} to slightly lower values of about −10. The samples with the highest silica contents may be affected by crustal contamination and their ε_{Nd} values could conceivably be up to 3 or 4 units lower than those of their parent magmas. However, this magnitude correction would not greatly affect the conclusions drawn below. The Mg# also shows no significant correlation with ε_{Nd} (Fig. 8b) which argues against a major role for crustal contamination as an explanation of the isotopic variations. If all of the samples are contaminated with crustal material to some degree, the net effect is to shift the ε_{Nd} scale, but the essential isotopic differences are preserved.

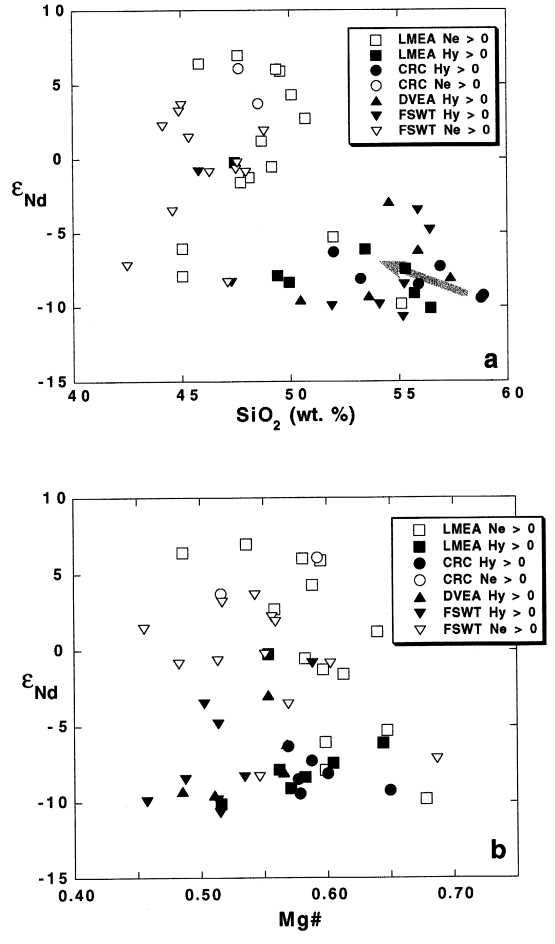

Fig. 8. (a) ε_{Nd} vs. silica content of samples from Table 1 plus samples from Feuerbach et al. (1993) labeled as FSWT. Shaded arrow shows approximate trajectory for a correction for crustal contamination. (b) ε_{Nd} vs. Mg# (= Mg/(Mg+Fe)). Most of the lavas have relatively low Mg# indicating they are differentiated, but there is no correlation of ε_{Nd} with Mg#.

9. Evidence for lithospheric and asthenospheric magma sources

The data suggest that the magma sources are composed principally of two components with distinct isotopic and trace element characteristics (Fig. 9). For the LMEA, CRC, and DVEA, the endmember that we associate with the lithosphere has a low value of ε_{Nd} (about -9 ± 2), high $^{87}Sr/^{86}Sr$ (0.7073 to 0.7097), and high and variable values of La/Nb (Fig. 9a and b). The asthenospheric endmember has characteristics that are similar to those of many ocean island basalts (PREMA; cf. Zindler and Hart, 1986) and generally attributed to typical upper mantle, at least the mantle as sampled other than at mid-ocean ridges. The asthenospheric magma source has high ε_{Nd} (about +8), low $^{87}Sr/^{86}Sr$ (0.703), and a low, well-defined value of La/Nb (0.7). The coherent correlation of the three parameters suggests that there are just two types of source materials, and that the intermediate values represent mixtures of the endmember compositions. All of the data plotted in Fig. 9a and b are from areas underlain by basement rocks with Nd model ages of 1.8 to 2.3 Ga (Fig. 5).

Based on the samples with high La/Nb, the ε_{Nd} of the lithospheric endmember in the Eastern Sierra and Mojave extensional areas is about -4 ± 2 (Fig. 9c and d). The corresponding values of $^{87}Sr/^{86}Sr$ are mostly in the range 0.705 to 0.707. These data provide the basis for distinguishing the Eastern Sierra Lithospheric mantle from that underlying the remainder of the study area (Fig. 5). The Nevada–Cali-

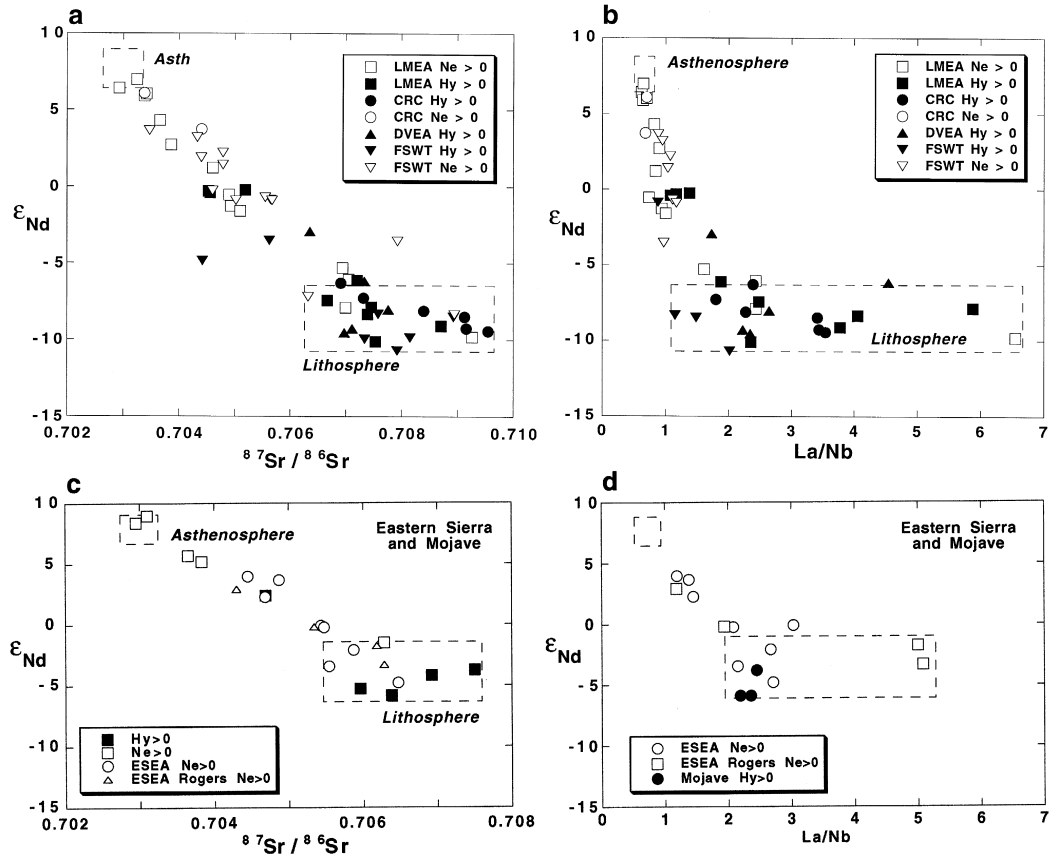

Fig. 9. (a) ε_{Nd} vs. $^{87}Sr/^{86}Sr$ for basalt samples from LMEA (Lake Mead Extensional Area), DVEA (Death Valley Extended Area), CRC (Colorado River Corridor) plus samples from Feuerbach et al. (1993) labeled as FSWT. Inferred compositions of lithospheric and asthenospheric mantle endmembers are shown. (b) ε_{Nd} vs. La/Nb for the same set of samples. Lithosphere-derived basalts are identified by the combination of low ε_{Nd} and high La/Nb. Two component mixing is inferred from the good correlation between ε_{Nd} and $^{87}Sr/^{86}Sr$. (c) ε_{Nd} vs. $^{87}Sr/^{86}Sr$ and (d) ε_{Nd} vs. La/Nb for basalt samples from ESEA (Eastern Sierra Extended Area) and the Mojave extensional area, showing inferred compositions of lithospheric and asthenospheric mantle. It is inferred that the eastern Sierra region and the Mojave Desert are underlain by a mantle lithosphere province that has higher ε_{Nd} than that underlying the extended regions immediately to the east (Fig. 5).

fornia area samples are not plotted; they span similar ranges of La/Nb, $^{87}Sr/^{86}Sr$ and ε_{Nd}, suggesting that the lithosphere is similar to that in the Eastern Sierra area. The NV/CA samples conform to the $^{87}Sr/^{86}Sr$-ε_{Nd} correlation (as in Fig. 9c), but show no correlation between La/Nb and ε_{Nd}.

10. Compositional trends and mantle stratigraphy

According to the model depicted in Fig. 2, there should be a broad relationship between basalt chemical composition and isotopic composition, reflecting the inferred mantle isotopic stratigraphy. If tholeiitic basalts are derived from depths of less than 50 km, it might be expected that very few tholeiitic basalts would have strong asthenospheric isotopic signatures. As shown in Fig. 10a, which exhibits data from LMEA, CRC, and DVEA, all of the lava samples with significant amounts of normative hypersthene have ε_{Nd} values lower than zero, and most have values lower than -5. All of the tholeiitic samples, except for a few post-extensional samples, therefore have strong lithospheric signatures as would be expected if the lithosphere seldom thinned to less

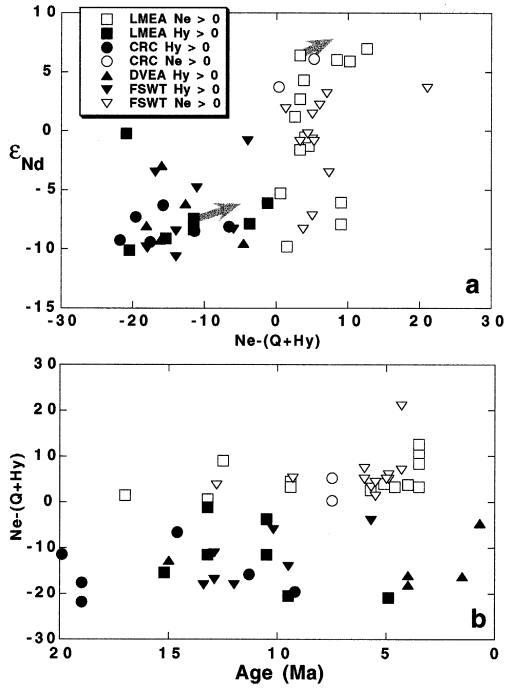

Fig. 10. (a) ε_{Nd} vs. normative Nepheline minus Hypersthene for basalt samples from LMEA (Lake Mead Extensional Area), DVEA (Death Valley Extended Area), CRC (Colorado River Corridor) plus samples from Feuerbach et al. (1993) labeled as FSWT. (b) Age vs. normative Nepheline minus Hypersthene, for the same samples.

than 50 km. The samples with 0 to 10% normative nepheline exhibit the complete range of ε_{Nd} from -10 to $+7$. These mildly alkaline lavas are derived from both the lithospheric and asthenospheric magma sources, and therefore indicate that the lithosphere was both thicker and thinner than 50–70 km during the extensional episode. Lavas with normative Ne contents $\geq 10\%$ (although there are only 3) have strong asthenospheric signatures. This is expected, considering that the depth of origin is in the range 80–100 km, close to the expected thickness of the lithosphere prior to extension, and that these lavas erupted near the end of the extensional episode when the lithosphere is expected to have been thinnest.

11. Temporal trends and lithosphere thinning

In this section, the Nd isotopic data are summarized for each of the geographical regions shown in Fig. 7. The data are compared to the model predictions (e.g. Fig. 4) for pure and distributed shear in those cases where there is sufficiently detailed information on the timing and magnitude of crustal extension. Inferences are drawn about the depth of the lithosphere–asthenosphere boundary as a function of time, based on the ages, Nd isotopic values, and the silica saturation of the basalts. For the purposes of mapping the isotopic data to lithosphere thickness, it is assumed that tholeiitic basalts (Hy $\pm$ Q normative) are derived from depths of less than 50 km, and that alkali basalts (Ne-normative) are derived from depths of 50 to 70 km. Therefore, for example, if alkali basalts have lithospheric isotopic signatures, it is inferred that the lithosphere is more than 70 km thick. If tholeiitic and alkali basalts have asthenospheric signatures, it is inferred that the lithosphere is less than 50 km thick. If alkali basalts have mixed isotopic signatures, it is inferred that the lithosphere is between 50 and 70 km thick. In a later section, the effects of changing these cutoff depths are considered. The inferred depth range of generation of basalts is similar to the depths estimated by Bradshaw et al. (1993) and Beard and Johnson (1997).

11.1. Lake Mead Extensional Area

In the southwestern part of the LMEA, alkalic basalts span the period of upper crustal extension between 15 and 5 Ma (Fig. 11a; open symbols). The alkalic lavas erupted before 12 Ma have strong lithospheric signatures ($\varepsilon_{Nd} = -5$ to -11), whereas those erupted at 6 to 4 Ma have strong asthenospheric signatures ($\varepsilon_{Nd} = -1$ to $+6$). Tholeiitic basalts were erupted mainly prior to 9.5 Ma and all show strong lithospheric signatures. The data suggest that prior to 12 Ma, the depth to the lithosphere–asthenosphere boundary was greater than 70 km, but by 10 Ma it was between 50 and 70 km. Hy-normative lava erupted at 5 Ma has an ε_{Nd} value (≈ 0) midway between those of the lithosphere and the asthenosphere. This suggests that the depth to the lithosphere–asthenosphere boundary at 5 Ma was less than 50 km. The lithospheric thinning inferred from the isotopic data for the LV/LM area is slower than expected for localized pure shear, but faster than expected for fully distributed shear.

The isotopic data for the northwestern part of this area (the Gold Butte–Grand Wash Trough area) does not span the full time of extension (Fig. 11a), but conforms to the inferences drawn from the southwestern lavas. In particular, the lavas erupted at about 5 Ma are transitional in character (either mildly Ne or mildly Hy normative), and they have ε_{Nd} values that are transitional between lithospheric and asthenospheric values. It is inferred that at 5 Ma the lithosphere–asthenosphere boundary must have been at a depth of less than 50 km. The ca. 4 Ma lavas all have very strong asthenospheric signatures ($\varepsilon_{Nd} = +2.5$ to $+7$), but are also more strongly Ne normative. The data from the 4 Ma basalts are consistent with a lithosphere thinned to >50 km, but do not require that there have been further thinning subsequent to 5 Ma.

11.2. Death Valley Extensional Area

Alkalic basaltic rocks from the DVEA record volcanic activity beginning at 12 Ma (Farmer et al., 1991) and continuing until <0.03 Ma (Farmer et al., 1989). The analyses from the central and western parts of the Death Valley region fall within a small range in composition: ε_{Nd} varies from -12 to -8, ε_{Sr} from $+35$ to $+45$, and trace element ratios Ba/Nb and La/Nb are relatively high (Fig. 11d and Table 1). In a roughly north–south oriented strip at the eastern margin of the Death Valley extended area, including Nye canyon (Farmer et al., 1989), the ε_{Nd} values for samples with ages between 10 and 4 Ma have clear asthenospheric character. The oldest sample shown in Fig. 11b is from the extreme southwestern part of the area, and appears to be derived from Eastern Sierra-type lithosphere based on the ε_{Nd} value and high La/Nb ratio.

The data shown in Fig. 11b imply that in the central and western Death Valley area the lithosphere remained >70 km thick throughout the period of extension, and the lithosphere is still thicker than 70 km at present. In the eastern margin of the area, the evidence suggests that the lithosphere thinned to 50–70 km in the Nye Canyon area by ca. 9 Ma, and perhaps to less than 50 km by 4 Ma in the southeastern part of the area. A comparison with the expected isotopic evolution (Fig. 11b) is based on the model of Wernicke and Snow (1998), in which the area covered by our sampling extends by a factor of $\beta \approx 2$ since 10 Ma. The model suggests that the asthenosphere–lithosphere transition for alkali basalts should occur between about 6 and 3 Ma. The data indicate that the transition occurred earlier along the eastern margin of the area, and did not occur at all in the central and western parts of the area.

11.3. Eastern Sierra Extensional Area

In this area, the ages of the lavas do not extend back to pre-extension time and the isotopic data show no clear changes as a function of age (Fig. 11c). There is evidence of a substantial asthenospheric component in alkalic lavas as early as 7 Ma. The youngest lavas span most of the range from the lithospheric to the asthenospheric values of ε_{Nd}. These data suggest that the lithosphere–asthenosphere boundary depth has been within the depth range of origin of alkali basalts (50–70 km) for the past 7 Ma. The isotopic (pure shear) trajectories shown (Fig. 11c) are based on the model of Wernicke and Snow (1998), assuming an extension factor of $\beta \approx 4$ since 10 Ma. This value of β is a maximum, as the amount of extension decreases from south to north by about 50%. The isotopic evidence for thinning is therefore roughly consistent with the pure shear model predictions for this area.

11.4. CRC area

Extension in the CRC slightly predated that in the Las Vegas area. The samples measured here are two pre-Peach Springs Tuff basalts near Kingman, AZ (>18.5 Ma; Nielson et al., 1990), and six basalts from the Mohave Mountains and Casteneda Hills area of west central AZ, which were erupted between 20 and 7.5 Ma (Nakata et al., 1990; Suneson and Lucchitta, 1983). The lavas erupted between 20 and 7.5 Ma are Hy normative. The oldest lavas from this area (age 20–22 Ma; data from Bradshaw et al., 1993) are alkaline and have moderately strong lithospheric signatures (Fig. 11c). The lithosphere thickness at 21 Ma is consequently inferred to be 50–70 km. The lavas erupted between 20 and 15 Ma have strong lithospheric signatures, but are also Hy normative, indicating that the lithosphere thickness was greater than 50 km at 15 Ma. The basalts erupted at

9 to 12 Ma, which include samples measured by Moyer and Esperança (1989), are Hy normative and show some asthenospheric isotopic character, indicating that the lithosphere–asthenosphere boundary

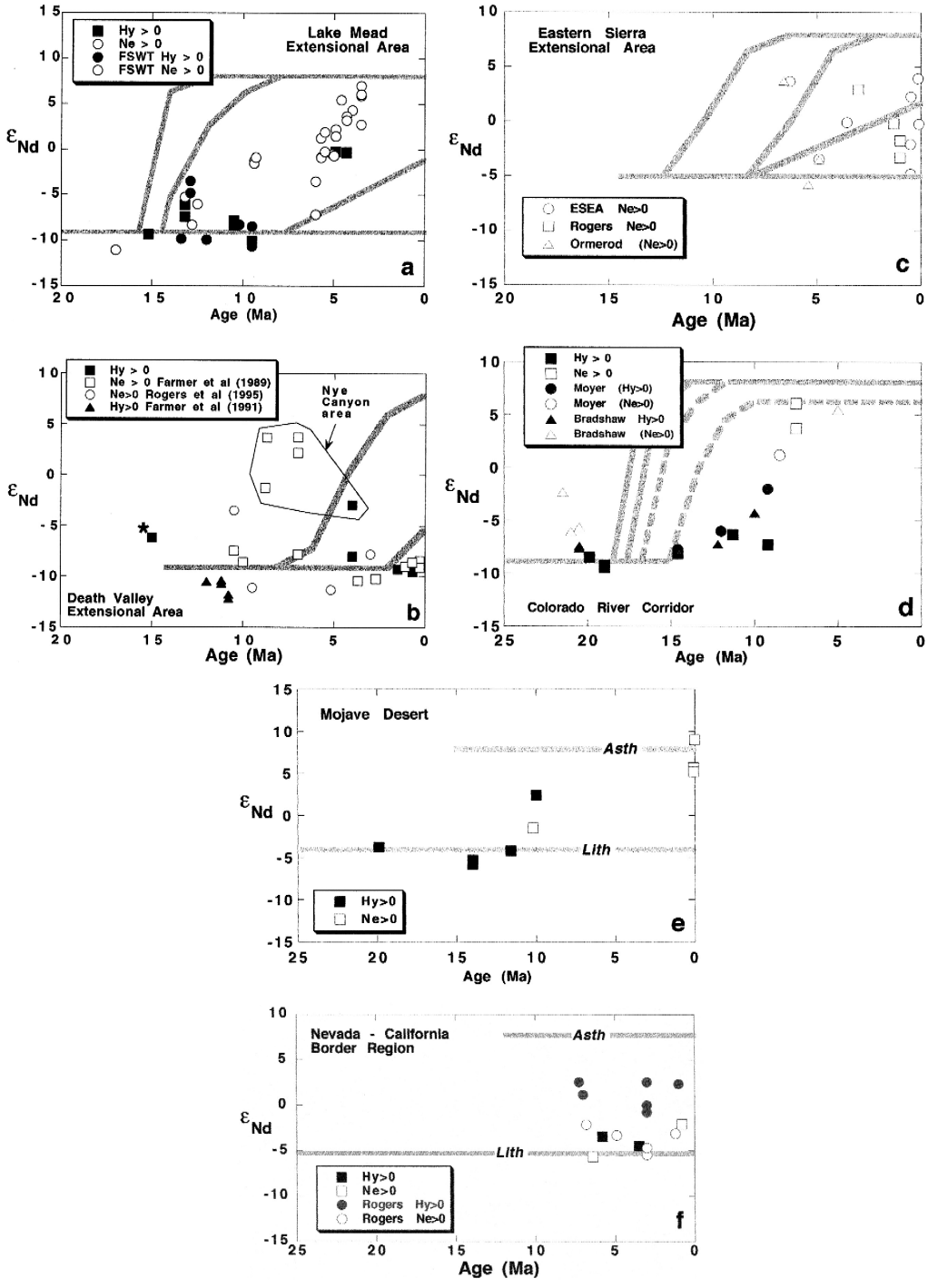

Table 3
Inferred depths to lithosphere–asthenosphere boundary

Region	Depth to lithosphere–asthenosphere boundary (km)					
	19–22	15–16	13–14	9–11	4–6 Ma	0 Ma
Lake Mead Extensional Area		> 70	50–70	50–70	< 50	
Eastern Death Valley (Nye Canyon area)				50–70	50–70	
Death Valley Extensional Area		> 70	> 70	> 70	> 70	> 70
Eastern Sierra Extensional Area					50–70	50–70
Colorado River Corridor	50–70	> 50		< 50		
Mojave Desert	> 50		> 50	< 50		< 50

was at depth of less than 50 km by 9 Ma. The post −9 Ma basalts are all Ne normative and have strong asthenospheric isotopic signatures ($\varepsilon_{Nd} = +1$ to +6), consistent with the lithosphere having been thinned to less than 50 km. The overall thinning of the lithosphere is clearly indicated by the contrast in isotopic composition between the > 20 Ma alkaline basalts and the < 9 Ma alkaline basalts. The approximate isotopic trajectories shown are based on the assumption of an extension factor of $\beta = 5$ and extension between 18.5 and 10 Ma. The observed lithospheric thinning is less than predicted by this model.

11.5. Mojave desert

Sparse data from volcanic rocks from the Mojave Desert show a general trend of increasing ε_{Nd} values with time (Fig. 11e). The hypersthene normative lavas with ages between 11.6 and 20 Ma have (eastern Sierra-type) lithosphere values of about −5, which suggests that the lithosphere thickness was greater than 50 km. A tholeiitic basalt at ca. 10 Ma has asthenospheric character ($\varepsilon_{Nd} = +2.4$; Musselwhite et al., 1989), suggesting that the lithosphere had thinned to less than 50 km by 10 Ma. Late Pleistocene alkali basalts of the Cima Volcanic Field, and Amboy and Pisgah craters, have strong asthenospheric signatures (Farmer et al., 1989, 1995; Glazner and Farmer, 1992) indicating that the lithosphere today is still 50 km or less in thickness.

11.6. California–Nevada border region

The northwestern region is underlain by accreted terrains of Phanerozoic age (Fig. 5) rather than Precambrian craton, and may be affected by subduction-zone magmatism. The observed relations between ε_{Nd}, chemical composition and age in the Nevada–California Border region, including Long Valley, are quite different from those of the other extensional areas. The hypersthene normative lavas have the strongest asthenospheric signatures (Fig. 11f), whereas the contemporaneous alkaline lavas have lithospheric signatures. Based on the isotopic signatures of the alkaline lavas, it appears that the lithosphere is still at least 70-km thick in this region. The hypersthene normative lavas may be related to

Fig. 11. ε_{Nd} vs. age for samples from each of the geographic areas shown in Fig. 7. Shaded lines indicate the expected pattern of variation for alkaline and tholeiitic basalts as predicted by lithospheric extension by pure shear and distributed shear as illustrated in Fig. 4. (a) LMEA, including data reported by Feuerbach et al., (1993) labelled as FSWT, (b) DVEA, including data from Farmer et al. (1989, 1991) and Rogers et al. (1995). Samples from the Nye Canyon area (see Fig. 7) are indicated. Oldest sample (with asterisk) corresponds to the sample locality shown with an asterisk in Fig. 7. The shaded lines on this plot represent the pure shear model only, and are calculated based on the extension model of Wernicke and Snow (1998). Curves for distributed shear would be the same as those shown in (a). (c) ESEA. This plot shows data from three samples reported by Ormerod (1988) for which ages were given. The shaded lines representing the pure shear model are calculated from the extension model of Wernicke and Snow (1998) assuming a total extension factor of $\beta = 4$. (d) CRC. The curves shown assume an extension factor of $\beta = 5$, and extension occurring between 18.5 and 10 Ma. (e) Mojave desert area. The ε_{Nd} values for asthenospheric and lithospheric magma sources are shown. Extension was mainly between 23 and 17 Ma. Data for the zero-age samples is from Farmer et al. (1989, 1995) and Glazner and Farmer (1992). (f) Nevada–California border area (NVCA). The ε_{Nd} values for asthenospheric and lithospheric magma sources are shown.

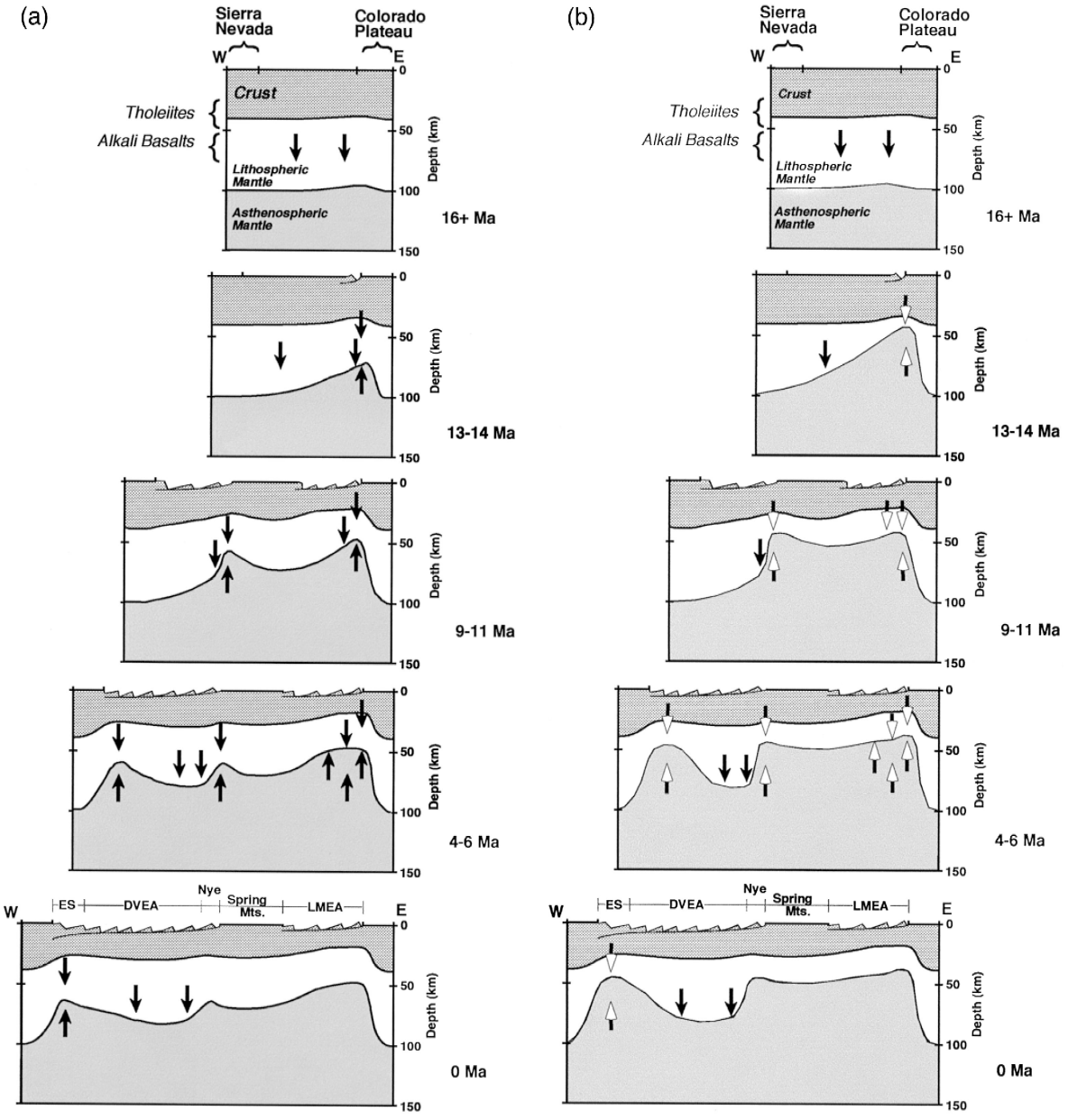

Fig. 12. Series of sections across the Basin and Range (along line A–A′ of Fig. 5) at different times prior to and during extension. Cross-section end points are fixed in the Sierra Nevada on the west and Colorado Plateau on the east, and the width of the intermediate region (Basin and Range) increases in successive cross-sections based on the estimated extension vectors of Wernicke et al. (1988). (a) Solid arrows indicate constraints on the depth to the lithosphere–asthenosphere boundary summarized in Table 2, which assume that the depth to the tholeiitic–alkaline boundary is 50 km and alkali basalts form between 50 and 70 km depth. The upper shaded layer is crust, the unshaded layer is lithospheric mantle, and the lower shaded layer is asthenospheric mantle. Labels on the 0 Ma cross-section refer to: LMEA — Lake Mead Extended Area; Nye — Nye Canyon region of eastern DVEA; DVEA — Death Valley Extended Area; ES — Eastern Sierra Extended Area. (b) Same as (a) but unfilled arrows show constraints on the depth to the lithosphere–asthenosphere boundary assuming that the depth to the tholeiitic–alkaline boundary is 40 km, and that alkali basalts with asthenospheric isotopic values form between 40 and 60 km depth.

the subduction environment, and carry asthenospheric signatures up from subduction zone depths, combined with high (but variable) La/Nb values characteristic of subduction zone magmas. This inversion of the normal depth–alkalinity relationship is evident in the basalts of the Long Valley area (Cousens, 1996; DePaolo, unpublished data) and in other continental volcanic arcs undergoing extension, such as the Colima Graben of the Trans-Mexican volcanic belt (Luhr, 1997).

12. Discussion: inferred patterns of lithospheric thinning

Constraints that can be placed on the depth of the lithosphere–asthenosphere boundary for five time intervals between 22 and 0 Ma are summarized in Table 3 and a series of cross-sections (Fig. 12a) along the transect A–A′ shown in Fig. 5. The cross-sections attempt to show the extension as well as the depth to the base of the lithosphere. As shown in the plates representing 13–14 and 9–11 Ma, lithospheric thinning beneath the LMEA and the eastern margin of the Death Valley region appears to have been substantial and concurrent with the extension of the upper crust. In contrast, as shown in the 9–11 and 4–6 Ma plates, the lithosphere was not significantly thinned beneath the central Death Valley Region even though there was a large amount of upper crustal extension. The 4–6 and 0 Ma plates show that crustal extension and lithospheric thinning were also contemporaneous in the Eastern Sierra area. The average thickness of the present-day lithosphere is inferred to be about 60 km under the entire extended area, which corresponds to thinning by a factor of about 1.67.

A second set of cross-sections is presented, representing different assumptions regarding the depth of origin of the basalts (Fig. 12b). For this set of sections, it is assumed that the depth of the alkali basalt–tholeiite transition is 40 km rather than 50 km. This might be a better approximation if the asthenospheric mantle is H_2O-poor, in which case both the alkaline and tholeiitic basalts with asthenospheric isotopic signatures could be formed at shallower depths than the corresponding magmas that have lithospheric signatures. This approach yields a similar overall pattern, but an average modern lithosphere thickness of about 50 km and a corresponding thinning factor of 2.0.

The patterns of lithospheric thinning inferred from the basalt geochemical data can be compared to models corresponding to pure and simple shear applied to the entire Colorado Plateau-to-Sierra Nevada transect (Fig. 13). Concurrent lithospheric thinning and upper crustal extensional deformation beneath the Lake Mead and Eastern Sierra areas, are consistent with the pure shear model. However, the pure shear model provides a poor fit to the data in the central part of the traverse. The lack of thinning beneath Death Valley is more consistent with the simple shear model and west-directed extension, but the simple shear model does not capture the geochemically inferred lithospheric thinning near the margin of the Colorado Plateau. In general, the total amount of lithospheric thinning indicated by the isotopic data is smaller than would be predicted by either of these models, and it is also more evenly distributed across the transect. The relatively even distribution of thinning supports models that incor-

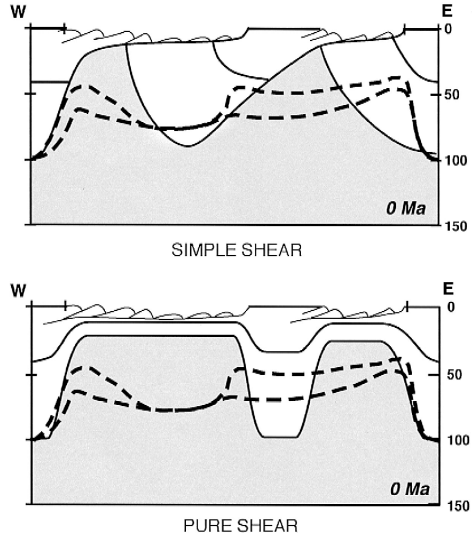

Fig. 13. Cross-sections showing present depths to the (chemical) lithosphere–asthenosphere boundary predicted from degree of upper crustal deformation based on end-member models for lithospheric extension: (a) simple shear and (b) pure shear. Cross-section line and scale are the same as Fig. 12 (0 Ma section). Heavy dashed lines are the lithosphere–asthenosphere boundary from Fig. 12a and b.

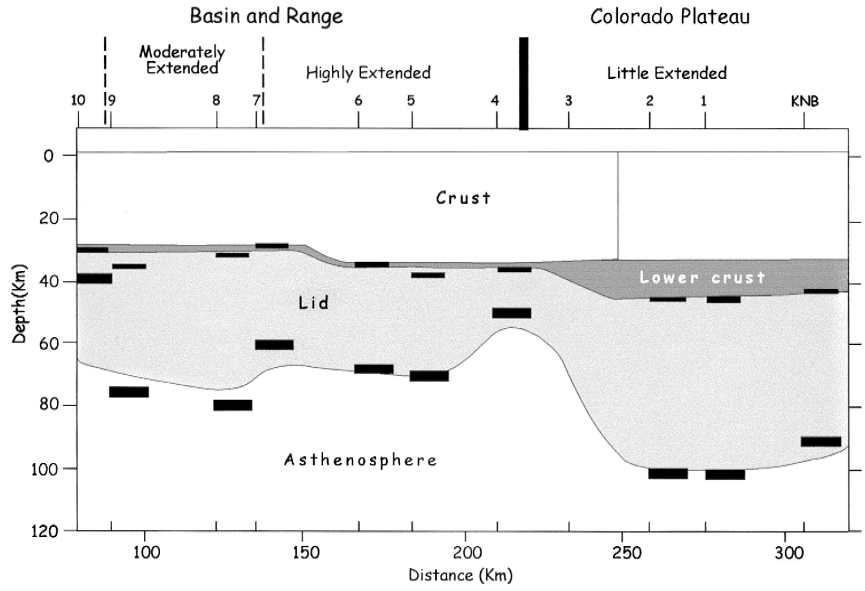

Fig. 14. Cross-section of the lithosphere constructed on the basis of seismic refraction data by Zandt et al (1995). Location of the cross-section is shown in Fig. 5.

porate flow in the lower lithosphere that distributes the shear strain laterally. The apparently limited overall thinning (a factor of 1.67 to 2.0 rather than 3) may or may not be significant, because it depends on the accuracy of several estimated values — the original thickness of the lithosphere, the depth of origin of the basalts, and the crustal stretching factor. The most recent estimate of overall crustal thinning (Wernicke and Snow, 1998) is in fact within the range of values inferred here from geochemical data.

Seismic refraction studies (Zandt et al., 1995; Fig. 14) provide a view of the present lithosphere thickness along an east–west transect (B–B′ in Fig. 5) that is located about 100 km north of Las Vegas. The seismic data apparently sense thin lithosphere under the eastern margin of the extended area, and place the lithosphere–asthenosphere boundary at a depth of about 55 km. This inferred structure is similar to that deduced from the isotopic data in the Lake Mead area. The seismic interpretation also shows thicker lithosphere (60–80 km) to the west, which is similar to the structure inferred from the isotopic data (Fig. 12). The lithosphere thickness inferred from geochemical data is somewhat smaller than that inferred from the seismic data. This difference is consistent with the observation that crustal thickness also decreases from $\geq$ 30 km in the region of cross-section B–B′ to about 20 km in the lower Colorado River area (Allenby and Schnetzler, 1983).

13. Sources of systematic error

Having carried the analysis through to completion, it is useful to review briefly possible sources of systematic error in estimating the depth to the lithosphere–asthenosphere boundary from basalt geochemistry. One issue is whether the estimated depths of origin of the lithosphere-derived basalts, by virtue of the requirement that the source region have water to facilitate melting, are offset relative to the depths inferred for asthenosphere-derived basalts. In the worst case, the depths inferred for the lithosphere-derived samples would need to be increased, whereas the depths inferred for the asthenosphere-derived samples might need to be decreased. This issue is addressed in Fig. 12b, although if the increased water content of the lithosphere is accompanied by an increase in alkalis, the two effects could offset one another. Another possible problem is that the lithospheric geochemical signature is held in sparsely distributed heterogeneities, so that as melting pro-

ceeds these heterogeneities are removed. In the later stages of extension, the disappearance of a lithospheric signal might then not require the lithosphere to be thinned, but only that the lithospheric enclaves with special geochemical characteristics be used up. This possibility would make our inferred thicknesses of the lithosphere minimum values, allowing the lithosphere to be thicker but not thinner than our estimated values.

14. Conclusions

Basalt lavas generated during intracontinental extension carry chemical and isotopic information on their depth of origin and the nature of the mantle material that constituted the magma source. The lithospheric mantle can be distinguished from the underlying asthenospheric mantle on the basis of isotopic and trace element patterns. In the southwest Basin and Range, the lithosphere has a low value of ε_{Nd} and elevated $^{87}Sr/^{86}Sr$ and La/Nb relative to the underlying asthenospheric mantle.

The isotopic and trace element characteristics of basaltic lavas erupted during the period of active extension in the Miocene show strong *temporal* changes. Lithospheric geochemical signatures predominate in the pre-extension and early extension basalts, and asthenospheric geochemical signatures typically predominate in the basalts erupted during the latter stages of extension. This pattern is most clearly evident in the data from the eastern margin of the extended area, in the region near Lake Mead and the lower Colorado River. The depth to the lithosphere–asthenosphere boundary can be inferred from the ε_{Nd}, $^{87}Sr/^{86}Sr$, and La/Nb values of the lavas as a function of age, and an estimate of the depth of origin of the magmas based on their silica saturation.

Two patterns are evident when the temporal relationship between upper crustal extension and basalt geochemistry are considered. In one case, thinning of the immediately subjacent lithosphere occurs contemporaneously with upper crustal extension. This relationship applies to the eastern margin of the extensional area near Lake Mead and the lower Colorado River, to a north–south oriented strip at the eastern margin of the Death Valley region, and to the western margin of the extensional area near the Sierra Nevada. In the other case, exemplified by most of the Death Valley region, strong extension of the upper crust ($\beta \approx 2$ to 4) is not reflected in thinning of the immediately subjacent lithosphere. In the regions where lithosphere thinning is inferred, it is both slower and smaller in magnitude than upper crustal extension.

The two patterns relating basalt geochemistry to upper crustal extension can be understood in terms of models for continental extensional strain (Fig. 1). The eastern and western margins of the extended area, where upper crustal extension and lithospheric thinning are co-located, conform in a general way to the pure shear and distributed shear models. In these models, the strain is distributed vertically in the lithosphere; the difference between the two models is in the magnitude of upper crustal vs. upper mantle thinning. The Death Valley area conforms to the simple shear model, where the region of lithospheric thinning is offset laterally from the region of upper crustal extension.

The inferred thickness of the present day lithosphere of the southwest Basin and Range varies from >70 to <50 km. For the east–west transect analyzed (37°N), the inferred average thinning of the lithosphere based on basalt geochemistry and an initial lithosphere thickness of 100 km is a factor of 1.67 to 2. This estimated factor is at the low end of the range of estimates for the stretching factor inferred from surface geology ($\beta = 2$ to 6), but is consistent with the present average thickness and inferred thinning of the crust. Overall, the agreement between the geochemical inferences and the structural interpretations is reasonably good. To fully reconcile the two data sets would require that either the extension factor was somewhat smaller than previously estimated, or that the initial lithosphere thickness for the extended area was greater than 100 km.

The approach described shows promise for elucidating the origins and geochemical characteristics of continental basalts, and for evaluating the deformation of the continental lithosphere during extension. Further refinement could come from a more quantitative treatment of magma generation and transport, although complications resulting from magma–crust interactions may ultimately limit the accuracy with which basalt geochemistry can be used to infer mantle properties and depth of origin.

Appendix A. Sample locations and age references

Number	Latitude (N)	Longitude (W)	Comments	Age reference
Lake Mead Extensional Area				
TPV-8	35°34.6	114°47.6	Lower Patsy Mine Fm.	Darvall et al. (1991)
TPV-2	35°47.8	114°47.3	Upper Patsy Mine Fm.	Darvall et al. (1991)
TDM-2	35°47.9	114°47.7	Davis Mine Fm.	Anderson et al. (1972)
TDM-5	35°47.9	114°47.7	Davis Mine (above TDM-2)	Anderson et al. (1972)
TDM-9	35°47.9	114°47.7	Davis Mine (above TDM-5)	Anderson et al. (1972)
TMV-1	36°10.0	114°43.6	Hill E. of Callville Bay Road	Feuerbach et al. (1991)
714-35	35°39.7	114°39.7	Dike, Hamblin Volcano (Collected by R.E. Anderson)	Anderson et al. (1972)
TMF-2	35°57.1	114°38.9	Hwy 93, S of Hoover Dam	Anderson et al. (1972)
TMF-5	35°48.3	114°38.1	Malpais Mesa	Feuerbach et al. (1993)
TMF-9	35°48.3	114°38.1	Several flows above TMF-5	Feuerbach et al. (1993)
TID-1	35°56.4	114°38.4	Dike east of Hwy 93	Anderson et al. (1972)
91-23	36°15.8	114°15.9	Quail Spr. Wash — top flow	Cole (1989)
91-24	36°16.2	114°16.5	Dike,W. of Quail Spr. Wash	Cole (1989)
91-25	36°15.9	114°15.0	Gold Butte — lowermost flow	Cole (1989)
91-26	36°22.2	114°01.1	St Thomas Gap	This work
91-27	36°39.3	113°47.4	Mud Mt. lowest flow	Cole (1989)
91-29	36°39.3	113°47.4	Mud Mt. highest flow of lower seq.	Cole (1989)
91-30	36°39.4	113°47.5	Mud Mt. dike; crosscuts upper seq.	Cole (1989)
91-31	36°39.4	113°47.6	Mud Mt.; lowest flow of upper seq.	Cole (1989)
91-32	36°39.4	113°47.6	Mud Mt.; highest flow, upper seq.	Cole (1989)
91-33	36°38.7	113°54.4	Cottonwood Wash, lowest flow	This work
91-34	36°38.7	113°54.4	Cottonwood Wash, highest flow	This work
Mojave Desert				
91-5d	34°44.8	116°14.53	Sleeping Beauty Mountains	Glazner (1986)
91-9	35°05.6	114°59.2	Piute Range	This work
91-12	35°6.8	114°58.0	Outlier in valley E of 91-9	This work
Colorado River Corridor				
91-14	34°46.5	114°21.3	N of Lake Havasu City, HWY 95	Nakata et al. (1990)
91-16	34°41.0	114°18.8	N of Lake Havasu City, HWY 95	Nakata et al. (1990)
91-49	34°25.0	113°40.5	Sample AP-19 of Suneson and Lucchitta (1979)	Suneson and Lucchitta (1979, 1983)

91-51	34°24.5	113°52.4	Plagioclase megacrysts	
91-52	34°21.1	113°48.6	Mesa capping basalt	Suneson and Lucchitta (1979, 1983)
91-53	34°27.6	113°56.3	Megacryst-bearing basalt	Suneson and Lucchitta (1979, 1983)
91-19	35°10.4	114°04.3	Pre-Peach Springs Tuff	Glazner (1986)
91-20	35°12.4	114°06.0	Pre-Peach Springs Tuff	Glazner (1986)
Southern Death Valley Region				
91-41	35°59.0	116°16.2	Hill-capping flow, Shoshone, CA	Pliocene (estimated)
91-42	35°58.3	116°22.4	Hill-capping flow W of Shoshone	Pliocene (estimated)
91-43	35°54.9	116°41.7	Funeral Fm., S. Death Valley(ppm)	Wright et al. (1984)
91-44	35°56.4	116°43.8	Cinder Hill, S Death Valley	Farmer et al. (1989)
91-47	35°41.8	116°49.2	Lost L. Drainage, S. Owlshead Mts.	Kistler and Peterman (1978)
Nevada–California Border Area				
91-54	37°49.0	117°39.6	Clayton Val., cinder cone	Albers and Stewart (1972)
91-55	37°50.1	117°40.0	Clayton Val., hill capping flows	This work
91-56	37°55.5	118°07.8	W. of Coaldale, ridge-capping flow	This work
91-57	37°57.6	118°20.8	W of Montgomery Pass	This work
91-58	38°16.8	119°09.4	Ridge N of Aurora Canyon Rd	Higgins and Evans (1983)
91-59	38°16.1	119°11.9	Ridge N of Aurora Canyon Rd	Higgins and Evans (1983)
91-60	38°10.0	119°07.3	Mt. Biederman Fm., S of Bodie	Chesterman and Gray (1975)
91-61	38°08.8	119°12.0	Rancheria Tuff Breccia	Al-Rawi, (1969)
91-62	37°37.9	118°51.8	Turnoff to Hot Creek, HWY 395	Bailey (1987)
Eastern Sierra Extensional Area				
91-63	37°05.6	118°15.9	Crater Mountain, Big Pine V.F.	Age (?)
91-64	37°01.2	118°13.9	Red Mountain, Big Pine V.F.	Age (?)
ECDP	36°20.8	117°29.5	Father Crowley overlook	This work
91-65	36°24.0	117°37.7	Darwin Plateau, Rd to Saline Val.	This work
91-66	36°23.6	117°48.4	S of HWY 190-136 junction	This work
91-67	36°16.3	117°45.6	Tbu of Duffield and Bacon (1981)	Duffield et al. (1980)
91-68	35°57.7	117°53.6	E of Little Lake, power line road	Duffield et al. (1980)
91-69	35°58.2	117°54.5	Near Fossil Falls	Duffield et al. (1980)
91-70	35°54.5	117°53.7	Ridge along power line	Duffield et al. (1980)

Acknowledgements

Brian Wernicke and R.E. Anderson helped get this project underway with a field trip to the Lake Mead area. Careful reviews by Brian Beard and Patricia Kempton helped to improve the manuscript. The research was supported by funds from the National Science Foundation (EAR-9004152, EAR-9304419, EAR-9614471) and by the Department of Energy, Office of Basic Energy Sciences, Geoscience Program under contract No. DE-AC03-76SF00098.

References

Al-Rawi, Y.T., 1969. Cenozoic history of the northern part of Mono Basin, California and Nevada. UC Berkeley, California PhD Thesis, 163 pp.

Albers, J.P., Stewart, J.H., 1972. Geology and mineral deposits of Esmerelda County, Nevada. Nev. Bur. Mines Geol., 78.

Allenby, R.J., Schnetzler, C.C., 1983. United States crustal thickness. Tectonophysics 93, 13–31.

Anderson, R.E., Longwell, C.R., Armstrong, R.L., Marvin, R.F., 1972. Significance of K–Ar ages of Tertiary rocks from the Lake Mead region, Nevada–Arizona. Geol. Soc. Am. Bull. 83, 273–288.

Armstrong, R.L., Higgins, R.E., 1973. K–Ar dating of the beginning of Tertiary volcanism in the Mojave Desert. Geol. Soc. Am. Bull. 84, 1095–1099.

Arndt, N.T., Christensen, U., 1992. The role of lithospheric mantle in continental flood volcanism: thermal and geochemical constraints. J. Geophys. Res. 97, 10967–10981.

Atwater, T., 1970. Implications of plate tectonics for the Cenozoic tectonic evolution of western North America. Geol. Soc. Am. Bull. 81, 3513–3536.

Asimow, P.D., Hirschmann, M.M., Stolper, E.M., 1997. An analysis of variations in isentropic melt productivity. Philos. Trans. R. Soc. London, Ser. A 355, 255–281.

Bailey, R.A., 1987. Geologic map of the Long Valley Caldera, Mono-Inyo-Craters volcanic chain, and vicinity, eastern California. USGS Map I-1933.

Bartley, J.M., Glazner, A.F., 1991. En echelon Miocene rifting in the southwestern United States and model for vertical-axis rotation in continental extension. Geology 19, 1165–1168.

Bayer, K.C., 1983. Generalized structural, lithologic and physiographic provinces in the fold and thrust belts of the United States. USGS Map, 1:2,500,000.

Beard, B.L., Glazner, A.F., 1995. Trace element and Sr and Nd isotopic composition of mantle xenoliths from the Big Pine volcanic field, California. J. Geophys. Res. 100, 4169–4179.

Beard, B.L., Glazner, A.F., 1998. Petrogenesis of isotopically unusual Pliocene olivine leucitites from Deep Springs Valley, California. Contrib. Mineral. Petrol. 133, 402–417.

Beard, B.L., Johnson, C.M., 1997. Hafnium isotope evidence for the origin of Cenozoic basaltic lavas from the southwestern United States. J. Geophys. Res. 102, 20149–20178.

Bennett, V.C., DePaolo, D.J., 1987. Proterozoic crustal history of the western United States as determined by Nd isotopic mapping. Geol. Soc. Am. Bull. 99, 674–685.

Block, L., Royden, L.H., 1990. Core complex geometries and regional scale flow in the lower crust. Tectonics 9 (4), 557–567.

Bradshaw, T.K., Hawkesworth, C.K., Gallagher, K., 1993. Basaltic volcanism in the southern Basin and Range: no role for a mantle plume. Earth Planet. Sci. Lett. 116, 45–62.

Buck, W.R., Martinez, F., Steckler, M.S., Cochran, J.R., 1988. Thermal consequences of lithospheric extension: pure and simple. Tectonics 7, 213–234.

Carmichael, I.S.E., Turner, F.J., Verhoogen, J., 1973. Igneous Petrology. McGraw-Hill, New York, 739 pp.

Chesterman, C.W., Gray, C.H., Jr., 1975. Geology of the Bodie Quadrangle, Mono and Tuolumne Counties, California. California Division of Mines and Geology Map Sheet Series, No. 22, 1:48,000 scale.

Cole, E.C., 1989. Petrogenesis of Late Cenozoic alkalic basalt near the eastern boundary of the Basin and Range: Upper Grand Wash Trough, Arizona and Gold Butte, Nevada. University of Nevada, Las Vegas, MS Thesis, 68 pp.

Cousens, B.L., 1996. Magmatic evolution of Quaternary mafic magmas at Long Valley caldera and the Devils Postpile, California — effects of crustal contamination on lithospheric mantle-derived magmas. J. Geophys. Res. 101, 27673–27689.

Daley, E.E., 1992. Temporal and spatial variations in composition of young mafic volcanic rocks of the southwestern Basin and Range: isotopic constraints on the relationship between thinning in the lithosphere and extensional deformation in the upper crust. PhD Thesis, U. California, Berkeley.

Daley, E.E., DePaolo, D.J., 1992. Isotopic evidence for contrasting upper crust and lower lithosphere strain histories during extension: SE Great Basin. Geology 20, 104–108.

Darvall, P., Gans, P.B., Lister, G.S., 1991. Normal faulting in the Eldorado mountains, SE Nevada. Geol. Soc. Am. Abstr. Programs 23, 17.

DePaolo, D.J., 1978. Study of magma sources, mantle structure and the differentiation of the earth using variations of $^{143}Nd/^{144}Nd$ in igneous rocks. PhD Dissertation, California Institute of Technology, 360 pp.

DePaolo, D.J., 1979. Estimation of the depth of origin of basic magmas: a modified thermodynamic approach and a comparison with experimental melting studies. Contrib. Mineral. Petrol. 69, 265–278.

De Voogd, B., Serpa, L., Brown, L., 1988. Crustal extension and magmatic processes: COCORP profiles from Death Valley and the Rio Grande Rift. Geol. Soc. Am. Bull. 100, 1550–1567.

Dickinson, W.R., 1981. Plate tectonics and the continental margin of California. In: Ernst, W.G. (Ed.), The Geotectonic Development of California. Rubey vol. 1 Prentice-Hall, Englewood Cliffs, NJ, USA, pp. 1–28.

Dickinson, W.R., Snyder, W.S., 1979. Geometry of triple junctions related to San Andreas transform. J. Geophys. Res. 84, 561–572.

Dodson, A., DePaolo, D.J., Kennedy, B.M., 1998. Helium isotopes in lithospheric mantle: evidence from tertiary basalts of the western U.S. Geochim. Cosmochim. Acta 62, 3775–3787.

Dokka, R.K., 1986. Patterns and modes of early Miocene crustal extension, central Mojave Desert, California. Geol. Soc. Am., Spec. Pap. 208, 75–95.

Dokka, R.K., 1989. The Mojave extensional belt of southern California. Tectonics 8 (2), 363–390.

Duffield, W.A., Bacon, C.R., Dalrymple, G.B., 1980. Late cenozoic volcanism, geochronology and structure of the Coso range, Inyo county, Califronia. J. Geophys. Res. 85, 2381–2404.

Duffield, W.A., Bacon, C.R., 1981. Geological map of the Coso Volcanic Field and adjacent areas, Inyo Co, CA, USGS Misc Investigations Series Map l-1200.

Eaton, G.P., 1982. The basin and range province: origin and tectonic significance. Annu. Rev. Earth Planet. Sci. 10, 409–440.1.

Farmer, G.L, 1988. Isotope geochemistry of Mesozoic and Tertiary igneous rocks in the western United States and implications for the structure and composition of the deep continental lithosphere. In: Ernst, W.G. (Ed.), Metamorphism and Crustal Evolution of the Western United States. Rubey vol. 7 Prentice-Hall, Englewood Cliffs, NJ, USA, pp. 87–109.

Farmer, G.L., DePaolo, D.J., 1983. Origin of Mesozoic and Tertiary granite in the western United States and implications for pre-Mesozoic crustal structure: 1. Nd and Sr isotopic studies in the geocline of the northern Great Basin. Geol. Soc. Am. Bull. 88, 3379–3401.

Farmer, G.L., Perry, F.V., Semken, S., Crowe, B., Curtis, D., DePaolo, D.J., 1989. Isotopic evidence on the structure and origin of subcontinental lithospheric mantle in southern Nevada. J. Geophys. Res. 94, 7885–7898.

Farmer, G.L., Broxton, D.E., Warren, R.G., Pickthorn, W., 1991. Nd, Sr, and O isotopic variations in metaluminous ash-flow tuffs and related volcanic rocks at the Timber Mountain–Oasis Valley caldera complex, SW Nevada: implications for the origin and evolution of large-volume silicic magma bodies. Contrib. Mineral. Petrol. 109, 53–68.

Farmer, G.L., Glazner, A.F., Wilshire, H.G., Wooden, J.L. et al., 1995. Origin of late cenozoic basalts at the cima volcanic field, Mojave Desert, California. J. Geophys. Res. 100, 8399–8415.

Faulds, J.E., Geissman, J.W., Mawer, C.K., 1990. Structural development of a major extensional accommodation zone in the Basin and Range province, northwestern Arizona and southern Nevada: implications for kinematic models of continental extension. Geol. Soc. Am., Mem. 176, 37–76.

Faulds, J.E., Geissman, J.W., Shafiqullah, M., 1992. Implications of Paleomagnetic data on Miocene extension near a major accommodation zone in the Basin and Range province, northwestern Arizona and southern Nevada. Tectonics 11 (2), 204–227.

Feuerbach, D.L., Smith, E.I., Shafiqullah, M., Damon, P.E., 1991. New K–Ar dates for late Miocene to early pliocene mafic volcanic rocks in the Lake Mead area, Nevada and Arizona. Isochron/West 57, 17–20.

Feuerbach, D.L., Smith, E.I., Walker, J.D., Tangeman, J.A., 1993. The role of the mantle during crustal extension: constraints from geochemistry of volcanic rocks in the Lake Mead area, Nevada and Arizona. Geol. Soc. Am. Bull. 105, 1561–1575.

Fitton, J.G., James, D., Kempton, P.D., Ormerod, D.S., Leeman, W.P., 1988. The role of lithospheric mantle in the generation of late Cenozoic basic magmas in the Western United States. J. Petrol., 331–349, Special Lithospheric Issue.

Fitton, J.G., James, D., Leeman, W.P., 1991. Basic magmatism associated with Late Cenozoic extension in the Western United States: compositional variations in space and time. J. Geophys. Res. 96 (B8), 13693–13711.

Fitzgerald, P.G., Fryxell, J.E., Wernicke, B.P., 1991. Miocene crustal extension and uplift in southeastern Nevada: constraints from fission track analysis. Geology 19, 1013–1016.

Foster, D.A., Miller, D.S., Miller, C.F., 1991. Tertiary extension in the Old Woman Mountains area, California: evidence from apatite fission track analysis. Tectonics 10, 875–886.

Gallagher, K., Hawkesworth, C., 1992. Dehydration melting and the generation of continental flood basalts. Nature 358, 57–59.

Gans, P.B., 1987. An open-system, two-layer crustal stretching model for the eastern Great Basin. Tectonics 6, 1–12.

Glazner, A.F., 1986. Stratigraphy, structure, and potassic alteration of Miocene volcanic rocks of the Sleeping Beauty area, Central Mojave Desert, CA. In: Nielsen, J.E., Glazner, A.F. (Eds.), Cenozoic Stratigraphy, Structure, and Mineralization in the Mojave Desert, GSA Cordilleran Section Guidebook, Trips 5 and 6. pp. 51–63.

Glazner, A.F., Bartley, J.M., 1984. Timing and tectonic setting of Tertiary low-angle normal faulting and associated magmatism in the southwestern United States. Tectonics 3, 385–396.

Glazner, A.F., Farmer, G.L., 1992. Production of isotopic variability in continental basalts by cryptic crustal contamination. Science 255, 72–74.

Green, D.H., 1971. Composition of basaltic magmas as indicators of conditions of origin: application to oceanic volcanism. Philos. Trans. R. Soc. London, Ser. A 268, 707–725.

Harry, D.L., Leeman, W.P., 1995. Partial melting of melt metasomatized subcontinental mantle and the magma source potential of the lower lithosphere. J. Geophys. Res. 100, 10255–10269.

Higgins, C.T., Evans, S.H. Jr., 1983. K–Ar dates of volcanic rocks in the western Bodie Hills, California. Isochron/West 36, 3–6.

Howard, K.A., John, B.E., 1987. Crustal extension along a rooted system of imbricate low-angle faults: Colorado River extensional corridor, California and Arizona. In: Coward, M.P., Dewey, J.F., Hancock, P.L. (Eds.), Continental Extensional Tectonics. Geological Society Special Publication vol. 28, pp. 299–311.

Johnson, C.M., 1991. Large scale crust formation and lithosphere modification beneath Middle to Late Cenozoic calderas and volcanic fields, Western North America. J. Geophys. Res. 96 (B8), 13485–13507.

Kempton, P.D., Fitton, J.G., Hawkesworth, C.J., Ormerod, D.S., 1991. Isotopic and Trace element Constraints in the composition and evolution of the lithosphere beneath the Southwestern United States. J. Geophys. Res. 96 (B8), 13713–13735.

Kistler, R.W., Peterman, Z.E., 1978. Reconstruction of crustal blocks of California on the basis of initial strontium isotopic compositions of Mesozoic granitic rocks. United States Geological Survey Professional Paper 1071, 17 pp.

Kushiro, I., 1996. Partial melting of a fertile mantle peridotite at high pressures: an experimental study using aggregates of diamond. In: Basu, A. (Eds.), Earth Processes: Reading the Isotopic Code. Am. Geophys. Union Geophys. Monogr. 95, pp. 109–122.

Langmuir, C.H., Klein, E., Plank, T., 1992. Petrological systematics of mid-ocean ridge basalts: constraints on melt generation beneath ocean ridges. Am. Geophys. Union, Geophys. Monogr. 71, 183–280.

Luedeke, R.G., Smith, R.L., 1981. Map showing distribution, composition, and age of Late Cenozoic volcanic centers in California and Nevada, USGS Misc. Investigations Series MAP I-1091-C.

Luhr, J.F., 1997. Extensional tectonics and the diverse primitive volcanic rocks in the western Mexican volcanic belt. Can. Mineral. 35, 473–500.

Lum, C.C.L., Leeman, W.P., Foland, K.A., Kargel, J.A., Fitton, J.G., 1989. Isotopic variations in continental basaltic lavas as indicators of mantle heterogeneity: examples from the western U.S. Cordillera. J. Geophys. Res. 94 (B6), 7871–7884.

McKenzie, D., Bickle, M.J., 1988. The volume and composition of melt generated by extension of the lithosphere. J. Petrol. 29, 625–679.

Menzies, M.A., 1989. Cratonic, circumcratonic, and mantle domains beneath the Western United States. J. Geophys. Res. 94 (B6), 7899–7915.

Menzies, M.A., Kyle, P.R., 1990. Continental volcanism: a crust–mantle probe. In: Menzies, M.A. (Ed.), Continental Mantle, Oxford Monographs on Geology and Geophysics no. 16. Clarendon Press, Oxford, pp. 157–177.

Moyer, T.C., Esperança, S., 1989. Geochemical and isotopic variations in a bimodal magma system: the Kaiser Spring Volcanic Field, Arizona. J. Geophys. Res. 94 (B6), 7841–7859.

Musselwhite, D.S., DePaolo, D.J., McCurry, M., 1989. The evolution of a silicic Magma system: isotopic and chemical evidence from the Woods Mountains Volcanic center, Eastern California. Contrib. Mineral. Petrol. 101, 19–29.

Nakata, J.K., Pernokas, M.A., Howard, K.A., Nielsen, J.E., Shannon, J.R., 1990. K–Ar and fission track ages (dates) of volcanic, intrusive, altered, and metamorphic rocks in the Mohave Mountains area, West Central Arizona. Isochron/West 56, 8–20.

Nelson, C.A., 1981. Basin and range province. In: Ernst, W.G. (Ed.), The Geotectonic Development of California. Rubey vol. 1 Prentice-Hall, Englewood Cliffs, NJ, USA, pp. 203–216.

Nielson, J.E., Lux, D.R., Dalrymple, G.B., Glazner, A.F., 1990. Age of the Peach Springs Tuff, Southeastern California and Western Arizona. J. Geophys. Res. 95 (B1), 571–580.

Ormerod, D.S., 1988. Late- to Post-Subduction Magmatic Transitions in the Western Great Basin, U.S.A. PhD, Dissertation, The Open University, UK, 313 pp.

Ormerod, D.S., Hawkesworth, C.J., Rogers, N.W., Leeman, W.P., Menzies, M.A., 1988. Tectonic and magmatic transitions in the Western Great Basin, USA. Nature 333 (26), 349–353.

Pakiser, L.C., 1989. Geophysics of the intermontane system. In: Pakiser, L.C., Mooney, W.D. (Eds.), Geophysical Framework of the Continental United States. Geological Society of America Memoir vol. 172, pp. 235–247.

Perry, F.V., Baldridge, W.S., DePaolo, D.J., 1987. The role of asthenosphere and lithosphere in the genesis of Late Cenozoic basaltic rocks from the Rio Grande Rift and adjacent regions of the Southwestern United States. J. Geophys. Res. 92, 9193–9213.

Perry, F.V., Baldridge, W.S., DePaolo, D.J., 1988. Chemical and isotopic evidence for lithospheric thinning beneath the Rio Grande Rift. Nature 332, 432–434.

Reid, M.R., Ramos, F.C., 1996. Chemical Dynamics of enriched Mantle in the Southwestern United States - Thorium Isotope evidence. Earth Planet. Sci. Lett., V138, 67–81.

Rogers, N.W., Hawkesworth, C.J., Ormerod, D.S., 1995. Late Cenozoic basaltic volcanism in the Western Great Basin, California and Nevada. J. Geophys. Res. 100, 10287–10301.

Schweig, E.S., 1984. Neogene tectonics and paleogeography of the southwestern Great Basin, California. PhD Dissertation, Stanford University, 207 pp.

Shackleford, T.J., 1980. Tertiary tectonic denudation of a Mesozoic–early Tertiary (?) gneiss complex, Rawhide Mountains, western Arizona. Geology 8, 190–194.

Smith, A.G., 1981. Subduction and coeval thrust belts, with particular reference to North America. In: McClay, K.R., Price, N.J. (Eds.), Thrust and Nappe Tectonics. pp. 111–124, Geological Society of London Special Publication no. 9.

Smith, R.B., Nagy, W.C., Julander, K.A., Viveiros, J.J., Barker, C.A., Gants, D.G., 1989. Geophysical and tectonic framework of the eastern Basin and Range–Colorado Plateau–Rocky Mountain transition. In: Pakiser, L.C., Mooney, W.D. (Eds.), Geophysical Framework of the Continental United States. Geological Society of America Memoir vol. 172, pp. 205–233.

Snow, J.K., Wernicke, B.P., 1989. Uniqueness of geological correlations: an example from the Death Valley extended terrain. Geol. Soc. Am. Bull. 101, 1351–1362.

Sonder, L.J., England, P.C., Wernicke, B.P., Christiansen, R.L., 1987. A physical model for Cenozoic extension of western United States. In: Conrad, M.P., Dewey, J.F., Hancock, P.L. (Eds.), Continental Extensional Tectonics. pp. 187–201, Geological Society Special Publication No. 28.

Spencer, J.E., Reynolds, S.E., 1986. Some aspects of the middle Tertiary tectonics of Arizona and southeastern California. Ariz. Geol. Soc. Dig. 16, 102–107.

Spencer, J.E., Reynolds, S.E., 1991. Tectonics of mid-Tertiary extension along a transect through west central Arizona. Tectonics 10, 1204–1221.

Stewart, J.H., 1975. Initial deposits in the Cordilleran Geosyncline: evidence of a Late Precambrian (< 850 m.y.) continental separation. Geol. Soc. Am. Bull. 83, 1345–1360.

Stewart, J.H., 1980a. Regional tilt patterns of late Cenozoic basin–range fault blocks, western United States. Geol. Soc. Am. Bull. 91, 460–464.

Stewart, J.H., 1980b. Geology of Nevada. pp. 1–136, Nevada Bureau of Mines Special Publication 4.

Suneson, N., Lucchitta, I., 1979. K–Ar ages of Cenozoic volcanic rocks, west-central Arizona. Isochron/West 24, 25–29.

Suneson, N., Lucchitta, I., 1983. Origin of bimodal volcanism, southern Basin and Range Province, west-central Arizona. Geol. Soc. Am., 1005–1019.

Takahashi, E., Kushiro, I., 1983. Melting of dry peridotite at high pressures and basalt magma genesis. Am. Mineral. 68, 859–879.

Wasserburg, G.J., Jacobsen, S.B., DePaolo, D.J., McCulloch, N.M.T., Wen, T., 1981. Precise determination of Sm/Nd ratios, Sm and Nd isotopic abundances in standard solutions. Geochim. Cosmochim. Acta 45, 2311–2323.

Watson, S., McKenzie, D.P., 1993. Melt generation by plumes: a study of Hawaiian volcanism. J. Petrol. 32, 501–537.

Wdowinski, S., Axen, G.J., 1992. Isostatic rebound due to tectonic denudation: a viscous flow model of a layered lithosphere. Tectonics 11 (2), 303–315.

Wernicke, B., 1985. Uniform-sense normal simple shear of the continental lithosphere. Can. J. Earth Sci. 22, 108–125.

Wernicke, B., 1990. The fluid crustal layer and its implications for continental dynamics. In: Salisbury, M.H., Fountain, D.M. (Eds.), Exposed Cross Sections of the Continental Crust. Kluwer Academic Publishing, Netherlands, pp. 509–544.

Wernicke, B., Axen, G.J., Snow, J.K., 1988. Basin and range extensional tectonics at the latitude of Las Vegas, Nevada. Geol. Soc. Am. Bull. 100, 1738–1757.

Wernicke, B.P., Christiansen, R.L., England, P.C., Sonder, L.J., 1987. Tectonomagmatic evolution of Cenozoic extension in the North American Cordillera. In: Conrad, M.P., Dewey, J.F., Hancock, P.L. (Eds.), Continental Extensional Tectonics. pp. 203–221, Geological Society Special Publication No. 28.

Wernicke, B., Snow, J.K., 1998. Cenozoic tectonism and central Basin and Range: motion of the Sierran–Great Valley block. Int. Geol. Rev. 40, 403–410.

Wright, L., Drake, R., Troxel, B.W., 1984. Evidence for the westward migration of severe Cenozoic extension, Southern Great Basin, CA. Geol. Soc. Am. Abstr. Programs 16, 701.

Zandt, G., Myers, S.C., Wallace, T.C., 1995. Crust and mantle structure across th Basin and Range–Colorado Plateau boundary at 37°N latitude and implications for Cenozoic extensional mechanism. J. Geophys. Res. 100, 10529–10548.

Zindler, A., Hart, S.R., 1986. Chemical geodynamics. Annu. Rev. Earth Planet. Sci. 14, 493–571.